ANNALS OF PHYSICS 182, 191–236 (1988)

Semi-empirical Effective Interactions for the 1*s*–0*d* Shell

B. A. BROWN

National Superconducting Cyclotron Laboratory and Department of Physics and Astronomy, Michigan State University, East Lansing, Michigan 48824

W. A. RICHTER

Physics Deparmtment, University of Stellenbosch, Stellenbosch 7600, South Africa

R. E. JULIES

Physics Department, University of the Western Cape, Private Bag X17, Bellville, C. P. 7530, South Africa

AND

B. H. WILDENTHAL

Department of Physics and Astronomy, University of New Mexico, Albuquerque, New Mexico 87131

Received December 7, 1987

Ground-state binding energies and excited-state energies of nuclei in the 1*s*–0*d* shell are analyzed in terms of a variety of two-body interactions. In addition to simple interactions such as the delta and surface-delta, we consider potentials of the finite-range, one-boson-exchange type for the central, tensor, and spin–orbit components of the interaction, with multipole terms added to the central part. The relative importance of these components, together with that of the antisymmetric spin–orbit component, is considered. The antisymmetric spin–orbit component is found to be the least important. Both density-dependent and density-indpendent interactions are considered. Our results favor a density-dependent form for the central and spin–orbit components. We develop a semi-empirical "best-fit" interaction based on a 14-parameter density-dependent two-body potential which reproduces 447 *sd*-shell binding-energy data to within an rms deviation between experiment and theory of 260 keV. This semi-empirical interaction is compared to typical *G*-matrix interactions as well as to the purely empirical interactions obtained by using two-body matrix elements or Talmi integrals as parameters of the fit.

0003-4916/88 $7.50

I. INTRODUCTION

The interaction between the nucleons in the nucleus is a crucial ingredient in all nuclear structure calculations. In the truncated bases which are always used in practice, one must introduce a mode-space-dependent effective interaction, $H = T + V$, which is a modification of the free-space nucleon–nucleon interaction. Much progress has been made in formally deriving such "theoretical" effective interactions from first principles, and they have been qualitatively successful in reproducing nuclear properties (see, for example, Refs. [1, 2]). However, the model wavefunctions which are most extensively and successfully used for the analysis of experimental data have been generated from empirical parameterizations of the effective interaction (see, for example, Refs. [3, 4]). There are many ways of making this parameterization, ranging from those that are strongly interaction-model dependent to those that are weakly interaction-model independent. The assumption of delta-function interactions is an example of the former, and the use of the two-body matrix elements themselves as parameters is an example of the latter. It is difficult to judge the relative efficacy of the diverse parameterization methods which have been used in the literature, because they typically have been used in isolation from one another and have been applied in different model spaces to different ranges of nuclei.

In this paper we present a unified and comprehensive study of the various methods for parameterizing the effective interaction. We do this by analyzing a large and consistent body of binding energies of ground and excited states of *sd*-shell nuclei with multi-particle wavefunctions obtained from the model-independent two-body matrix element (TBME) parameterization of Wildenthal (Ref. [5]). These wavefunctions serve to provide the coefficients (one- and two-body transition densities) which relate the total experimental binding energy data to linear combinations of one- and two-body matrix elements and hence to the details of the assumed two-body interactions. They span the complete "$0\hbar\omega$" model space, that is, the complete set of multi-particle configurations built out of the $0d_{5/2}$–$1s_{1/2}$–$0d_{3/2}$ orbitals. In Section II.A, general aspects of the least-squares fitting procedures used for that work are described. The specific assumptions and results pertaining to the *sd*-shell TBME parameterization are presented in Section II.C.

We investigate a wide variety of semi-empirical effective interactions. Our main goal is to provide some guidance for future large-basis shell-model calculations in which the effective interaction is not, a priori, given and for which the TBME parameterization is not practical. A secondary goal is to determine how the empirically optimal effective interactions differ from those derived from first principles.

The TBME parameterization has been successful in the *sd* shell because the number of input data (e.g., the 447 binding-energy data of Ref. [5]) is much larger than

the number of independent two-body matrix elements. For larger model spaces in heavier nuclei, the number of independent matrix elements increases relative to the number of data, and the model-independent TBME fit can no longer be used. There are many alternative ways of limiting the number of parameters. In this paper we explore these alternatives with regard to the *sd*-shell data set.

One of the key elements of our analysis is the transformation of the *jj*-coupled TBME into an *LS*-coupled representation, in which the various components of the interaction (central, tensor, spin–orbit, and antisymmetric spin–orbit) can be explicitly separated. This spin-tensor transformation is described in Section II.B. This is a unique transformation and it makes no assumptions about the interaction other than the fundamental one that it is based on a two-body operator.

Any attempt to limit the number of parameters which define the interaction makes some assumptions, either implicit or explicit, concerning the parts of the interaction which are not varied. For example, one often simply sets these parts to zero; as an alternative they could be set equal to *G*-matrix values. We explore both possibilities in this work. If the effective interaction is derivable from a potential which depends only on the relative and center-of-mass coordinates between two nucleons in the nucleus, then it is easy to show that the antisymmetric spin–orbit (ALS) component must vanish. The consequences of a vanishing ALS component are discussed in Section II.D. As we will show, little is lost by setting this component equal to zero, and essentially all of the fits discussed in this work will be made under the assumption that the ALS component vanishes.

The main body of this work consists of examining the consequences of placing various restrictions on the specifications of the central, tensor, and spin–orbit components. From the spin-tensor transformation, each of these components can be treated essentially independently by using the method described in Section II.B.

Potential models for the effective interaction are discussed in Section III. We start with a review of the Talmi–Moshinsky transformation in Section III.A. Features of the density dependence are discussed in Section III.B. The model-independent form for the potential models in terms of Talmi integrals is presented in Section III.C. In Section III.D, we present some results from phenomenological parameterizations based on fits to global nuclear properties and from microscopic parameterizations based on *G*-matrix elements derived from nucleon–nucleon potentials. Details of the *G*-matrix potential of Hosaka *et al.* (Ref. [6]) are given in Section III.E. Multipole interactions are discussed in Section III.F.

Results are discussed in Section IV, broken down into three categories: Section IV.A, the results obtained from "model-independent" methods; Section IV.B, the results obtained from "simple" potential models; and Section IV.C, the results obtained from the more complete potential models. In Section IV.D we select a "best-fit" interaction and examine some the remaining assumptions which go into its determination. The summary and conclusion together with some comments on future directions are presented in Section V.

II. Model-Independent Methods for the Effective Interaction

II.A. *General Fitting Methods*

In the single-particle basis of the shell model, the matrix element of the Hamiltonian $H = T + V$ between given multi-particle Slater determinants $|k\rangle$ and $|k'\rangle$ (m-scheme states) can be expressed in terms of a summation over the product of the one-body transition density, OBTD, with the single-particle energy, SPE, plus the product of the two-body transition density, TBTD, with the two-body matrix element, TBME,

$$\langle k\,|H|\,k'\rangle = \sum_i \mathrm{OBTD}(i,k,k')\,\mathrm{SPE}(i) + \sum_j \mathrm{TBTD}(j,k,k')\,\mathrm{TBME}(j), \tag{1}$$

where the label k stands for all quantum numbers needed to specify the multi-particle wavefunction and the indices i and j stand for all quantum numbers needed to specify the SPE and the TBME, respectively.

In a spherical basis with good isospin one can construct linear combinations of m-states which have definite spin J_k and isospin T_k, and the matrix elements have the form

$$\mathrm{SPE}(i) = \langle a_i|\ T\ |a_i\rangle \tag{2}$$

$$\mathrm{TBME}(j) = \langle a_j b_j JT|\ V\ |c_j d_j JT\rangle, \tag{3}$$

where a is shorthand for the quantum numbers (n_a, l_a, j_a) of the single-particle orbits, etc. For the *sd* shell the single-particle energy in Eq. (2) contains the contribution from the two-body interaction between the *sd*-shell orbits and the $0s$–$0p$ core, in addition to the kinetic energy. In a spherical basis, the OBTD and TBTD can be represented in terms of JT-coupled creation and annihilation operators (Ref. [7]).

An eigenfunction $|K\rangle$ is given in terms of a linear combination of Slater determinants

$$|K\rangle = \sum_k \alpha_k\,|k\rangle, \tag{4}$$

where the coefficients α_k are obtained by diagonalizing the matrix $\langle k|\ H\,|k'\rangle$. The eigenenergies can then be expressed in terms of linear combinations of the one- and two-body matrix elements

$$\langle K|\ H\,|K\rangle = \sum_i \mathrm{OBTD}(i,K)\,\mathrm{SPE}(i) + \sum_j \mathrm{TBTD}(j,K)\,\mathrm{TBME}(j), \tag{5}$$

where

$$\mathrm{OBTD}(i,K) = \sum_{k,k'} \alpha_k \alpha_{k'}\,\mathrm{OBTD}(i,k,k')$$

and

$$\mathrm{TBTD}(j, K) = \sum_{k,k'} \alpha_k \alpha_{k'} \, \mathrm{TBTD}(j, k, k'). \tag{6}$$

The OBTD(i, K) and TBTD(i, K) depend on H since the α_k depend on H.

The TBME could be taken as the parameters in the fit. Alternatively, the TBME may be expressed in terms of linear combinations of terms representing the various assumed parts or components of the interaction. This in general will take the form of a summation over products of a strength parameter, SP, times a coefficient, TBMECOMP, which represents the amount of the specified component in a particular TBME;

$$\mathrm{TBME}(i) = \sum_j \mathrm{SP}(j) \, \mathrm{TBMECOMP}(i, j), \tag{7}$$

where SP(j) is the strength of the given component. Then we have in place of Eq. (5)

$$\langle K| \, H \, |K\rangle = \sum_i \mathrm{OBTD}(i, K) \, \mathrm{SPE}(i) + \sum_j \mathrm{GTBTD}(j, K) \, \mathrm{SP}(j), \tag{8}$$

where GTBTD is a "generalized" two-body transition density given by

$$\mathrm{GTBTD}(j, K) = \sum_m \mathrm{TBTD}(m, K) \, \mathrm{TBMECOMP}(m, j). \tag{9}$$

In this work Eq. (8) will be used to obtain fits to the spin-tensor components of the interaction discussed in Section II.B and will also be used to obtain fits to various models for the interactions discussed in Section III.

The general fit method consists of the following steps:

(1) choice of some resonable starting Hamiltonian and calculation of the matrix elements $\langle k| \, H \, |k'\rangle$ and the resulting eigenfunctions $|K\rangle$,

(2) calculation of the OBTD(i, K) and TBTD(i, K),

(3) determination of new values of the SPE and TBME by making a linear least-squares fit to the experimental binding energies, substituted in place of the quantities $\langle K| \, H \, |K\rangle$ on the left-hand side of Eq. (8).

(4) from these new values of SPE and TBME, recalculation of the matrix elements $\langle k| \, H \, |k'\rangle$ and the eigenfunctions.

This sequence is reiterated until the values of SPE and TBME stabilize. The rate of convergence to stability depends upon the quality of the starting Hamiltonian.

Rather than directly solving the least-squares-fit matrix containing the Hamiltonian parameters and experimental energies as a set of linear equations, the matrix can be diagonalized. The eigenvectors from this diagonalization are linear

combinations of the Hamiltonian parameters which are uncorrelated one from another with respect to the data set. We will refer to this method, developed in Ref. [8], as the linear combination (LC) fit method. Details of this method, referred to as the diagonal matrix correlation method, are also given in Ref. [7].

The eigenvalues from this diagonalization give a measure of how well the data set fixes each of these combinations of parameters. This permits the variation of only the "well-determined" linear combinations of parameters while "poorly determined" combinations are held fixed at some assume values. Working with this subset of "well-determined," uncorrelated Hamiltonian parameters instead of the ordinary representation makes the adjustment and iteration procedure much more efficient and allows better control over, and insight into, the fitting process. In the iteration procedure the rate of convergence to stability depends on the cutoff between the "well-determined" and the "poorly determined" parameters, as well as on the type of constraints placed upon the "poorly determined" parameters. The complete specification of the linear-combination fit method thus must include specifying the number of parameters varied and what interaction (if any) is used in place of those linear combinations of parameters which are not varied.

The most general parameterization of the effective shell-model interaction can be made by choosing the SPE and TBME themselves as the parameters. We will refer to this case as the model-independent (MI) fit method. In the case of only one orbit in the model space, there are only a few TBME and these can often be easily related directly to the energies of the states of the two-particle spectra. In those cases where one shell-model orbit is relatively isolated from the others this method works rather well, in the sense that the multi-particle energy levels are well reproduced by the TBME obtained from the two-particle spectrum. One of the best examples of this is found in the $0f_{7/2}$ shell region (Refs. [9, 10]).

For model spaces with more than one active orbit there are many more TBME, and there is no longer a direct correspondence between single TBME and individual energy levels of the two-particle systems. By a consideration of the multi-particle spectra, additional information can be obtained which helps to constrain the values of the TBME. The *p*-shell work of Cohen and Kurath (Ref. [11]) was one of the first successful applications of the MI method in the multi-orbit case; there are 15 independent TBME in this case. For heavier nuclei the number of TBME rapidly increases and the LC method becomes essential. In Section II.C we discuss Wildenthal's application (Ref. [5]) of the LC method to the *sd*-shell nuclei in some detail.

We use the following standard definitions for the rms deviation, RMS, and goodness of fit, χ,

$$\mathrm{RMS}^2 = \sum_i^{N_d} [E_i(\mathrm{exp}) - E_i(\mathrm{th})]^2 / N_\mathrm{d}$$

$$\chi^2 = \sum^{N_\mathrm{d}} \{[E_i(\mathrm{exp}) - E_i(\mathrm{th})]/\Delta_i(\mathrm{exp})\}^2/(N_\mathrm{d} - \mathrm{N_p}),$$

where $E(\text{exp})$ are the experimental binding energies, $\Delta(\text{exp})$ are the experimental uncertainties, $E(\text{th})$ are the fitted theoretical binding energies, N_d is the number of data, and N_p is the total number of varied parameters in the least-squares fit.

II.B. *The Spin-Tensor Transformation*

Two-body matrix elements of the effective interaction can be interpreted in terms of the basic physics of the particle–particle interaction more readily in the representation of the LS coupling scheme than of the jj coupling scheme, the latter being the representation generally employed for shell-model calculations. The LS coupling scheme permits a spin-tensor transformation of the two-body matrix elements (Refs. [12, 13]). This method has been used in the analysis of effective interactions in the p shell (Ref. [14]) and in the sd shell (Refs. (15, 16]). The transformation can be used to decompose a given set of jj-coupled TBME into various interaction components as was done in (Ref. [16]). Alternatively, this transformation can be used to provide the coefficients in Eq. (7). This makes it possible to carry out the least-squares fits in terms of the more physically meaningful LS-coupled components of the interaction.

The two-body interaction can be written in the form

$$V=\sum_p V_p=\sum_p U^p\cdot X^p, \tag{10}$$

where the operators U and X are irreducible tensors of rank p in the space and spin coordinates, respectively. (The index p written as a superscript indicates the tensor rank of the operator, whereas written as a subscript it simply indicates a label.) Interaction components are specified by $p=0$ for central, $p=1$ for spin–orbit, and antisymmetric spin–orbit, and $p=2$ for tensor. The LS-coupled matrix elements of a given component V_p are related to the LS-coupled matrix elements of the total interaction by

$$\begin{aligned}&\langle ABLSJ'T|\,V_p\,|CDL'S'J'T\rangle\\&\quad=(-1)^{J'}(2p+1)\begin{Bmatrix}L & S & J'\\ S' & L' & p\end{Bmatrix}\sum_J(-1)^J(2J+1)\begin{Bmatrix}L & S & J\\ S' & L' & p\end{Bmatrix}\\&\qquad\times\langle ABLSJT|\,V\,|CDL'S'JT\rangle.\end{aligned} \tag{11}$$

These LS-coupled matrix elements are linear combinations of the jj-coupled matrix elements,

$$\begin{aligned}&\langle ABLSJT|\,V\,|CDL'S'JT\rangle\\&\quad=[(1+\delta_{AB})(1+\delta_{CD})]^{-1/2}\sum_{j_a,j_b,j_c,j_d}\begin{bmatrix}l_a & \frac{1}{2} & j_a\\ l_b & \frac{1}{2} & j_b\\ L & S & J\end{bmatrix}\begin{bmatrix}l_c & \frac{1}{2} & j_c\\ l_d & \frac{1}{2} & j_d\\ L' & S' & J\end{bmatrix}\\&\qquad\times[(1+\delta_{ab})(1+\delta_{cd})]^{1/2}\langle abJT|\,V\,|cdJT\rangle,\end{aligned} \tag{12}$$

where A is shorthand for the set of quantum numbers (n_a, l_a) and a is shorthand for the set (n_a, l_a, j_a), etc. The two-body matrix elements in these expressions are normalized and antisymmetrized. The large square bracket is the LS-to-jj transformation coefficient (Ref. [17]).

All of the J' dependence in the LS-coupled matrix element is provided trivially by the first $6-j$ coefficient in Eq. (11). For the tabulations and figures we use a value of J' which is the maximum allowed by the vector coupling of L to S and L' to S'.

Conversely, the jj-coupled matrix elements can be expressed as linear combinations of the spin-tensor matrix elements. This provides the transformation for making the least-squares fit (discussed in Section II.A) directly in terms of the spin-tensor components. Specifically:

$$\begin{aligned}\langle abJT|\, V\,|cdJT\rangle &= \sum_{L,S,L',S'} [(1+\delta_{ab})(1+\delta_{cd})]^{-1/2}[(1+\delta_{AB})(1+\delta_{CD})]^{1/2} \\ &\times \begin{bmatrix} l_a & \frac{1}{2} & j_a \\ l_b & \frac{1}{2} & j_b \\ L & S & J' \end{bmatrix} \begin{bmatrix} l_c & \frac{1}{2} & j_c \\ l_d & \frac{1}{2} & j_d \\ L' & S' & J' \end{bmatrix} \sum_p (-1)^{J-J'} \begin{Bmatrix} L & S & J \\ S' & L' & p \end{Bmatrix} \begin{Bmatrix} L & S & J' \\ S' & L' & p \end{Bmatrix}^{-1} \\ &\times \langle ABLSJ'T|\, V_p\,|CDL'S'J'T\rangle. \end{aligned} \tag{13}$$

The TBMECOMP(i, j) needed in Eq. (7) are given by the individual coefficients of the matrix elements in the above summation corresponding to a given set of jj-coupled quantum numbers $i=(a, b, c, d, J, T)$ and LS-coupled quantum numbers $j=(A, B, C, D, L, S, L', S', p, J', T)$. (When $L\neq L'$ or $S\neq S'$, care must be taken to include all possible partial sums over the nonunique combinations of L and S.)

We note that the matrix elements evaluated with all combinations of the spin–orbit pairs of orbit $(j=l\pm\frac{1}{2})$ are needed to make the spin-tensor decomposition in Eq. (11). However, the spin-tensor transformation of Eq. (13) can be used even if only a subset of this complete set is being considered.

II.C. *The sd-shell* W *Interaction*

The linear combination method has been used by Wildenthal (Ref. [5]) to obtain a specific interaction and the related set of sd-shell wavefunctions. We will refer to this interaction as the "W" interaction. Since our interactions are obtained with the same set of OBTB and TBTD which were used to obtain the W interaction, in this section we discuss the assumptions that went into this determination and show some results. Then, in preparation for the application of model-dependent interactions in Sections III and IV, we discuss in Section II.D the general results obtained from the spin-tensor transformation, and in particular, the role of the antisymmetric spin–orbit component.

The assumptions that went into the determination of the W interaction are as follows:

(1) The wavefunctions have good isospin. The Coulomb energy part of the experimental binding energies were removed in an approximate manner by subtracting the estimates based on displacement energies determined from pairs of analogue states. Details are given elsewhere (Refs. [8, 18]). Since the typical state dependence of the displacement energies for *sd*-shell nuclei is comparable to or smaller than the rms deviation in the fit discussed below, this assumption should be adequate.

(2) The TBME values retained for the poorly determined linear combinations in the fit were the renormalized G-matrix elements of Kuo (Ref. [19]).

(3) The TBME have a simple mass dependence, given by

$$\langle V\rangle(A) = \langle V\rangle(A=18)(A/18)^{-0.3}. \tag{14}$$

This mass dependence comes about because the basis states are assumed to be mass dependent. In principle, the basis states for an infinite model space, and hence the TBME, can be considered to be independent of mass. However, in practice, the truncation to the *sd* model space necessitates the introduction of a mass dependence. For example, if harmonic-oscillator radial wavefunctions with $\hbar\omega$ proportional to $A^{-1/3}$ are assumed, the TBME for a delta-function interaction vary as $(\hbar\omega)^{3/2}$ or $A^{-1/2}$. A longer-ranged potential gives a smaller mass dependence. For example, the TBME for a Coulomb interaction vary as $(\hbar\omega)^{1/2}$ or $A^{-1/6}$. Hosaka *et al.* (Ref. [6]) have found that the bare G-matrix interaction in the *sd* shell gives an average mass dependence of $A^{-0.25}$, with some scatter depending upon the channel (i.e., the various p, S, and T combinations in Table IV).

The empirical need for a mass dependence could be seen from the work of Chung (Ref. [8]), which was the immediate precursor to the work of Wildenthal. Two different sets of TBME were required: one for the lower part ($A=16-28$) of the *sd* shell and another for the upper part ($A=28-40$). In the succeeding work which developed the W interaction it was then found (Ref. [5]) that these "lower" and "upper" interactions could be unified in the fit by introducing the mass dependence given by Eq. (14).

(4) The SPE are mass independent. In principle, these could also be mass dependent, for the same reasons mentioned above (although it is more complicated than that for the TBME since there is a cancellation between potential and kinetic energy terms). Empirically, however, if a mass dependence is introduced for the SPE in the MI fit, the χ^2 of the fit is essentially unchanged, indicating that there are linear combinations of the *sd*-shell TBME which are strongly correlated with the mass-dependent SPE.

(5) The experimental data set to which the W interaction was fitted in the last iteration consisted of the binding energies for 447 ground and excited states of *sd*-shell nuclei. The range of nuclei considered is indicated in Table I, where the 447 states considered are broken down into their mass and isospin distribution. The relative lack of data in the middle of the shell reflects the fact that the dimensions of

TABLE I

Breakdown of the 447 Experimental *sd*-Shell Binding-Energy Input Data into Their Nuclear Mass Number (A) and Isospin (T) Values

A	$2T$	Number of data	A	$2T$	Number of data	A	$2T$	Number of data
17	1	3	25	1	7	32	0	13
18	0	6	25	3	4	32	2	19
18	2	4	25	5	1	32	4	4
19	1	13	26	0	9	33	1	16
19	3	8	26	2	4	33	3	7
20	0	9	26	4	1	33	5	1
20	2	13	26	6	1	34	0	13
20	4	4	27	1	4	34	2	12
21	1	14	27	3	3	34	4	3
21	3	6	27	5	1	35	1	17
21	5	1	28	0	9	35	3	5
22	0	16	28	2	2	35	5	1
22	2	23	28	4	1	36	0	7
22	4	1	28	6	1	36	2	11
22	6	1	29	1	3	36	4	3
23	1	17	29	3	2	37	1	8
23	3	11	29	5	1	37	3	4
23	5	1	29	7	1	38	0	4
24	0	21	30	0	10	38	2	3
24	2	19	30	2	5	39	1	3
24	4	5	30	4	1			
			30	8	1			
			31	1	15			
			31	3	7			
			31	5	1			
			31	9	1			

the mid-shell matrices are larger and that, consequently, the TBTD calculations needed for each iteration become too time-consuming.

With these assumptions, the W interaction was determined from five iterations of the linear-combination least-squares-fit method (Section II.A) starting with OBTD and TBTD obtained from the Chung wavefunctions for $A = 17$–24 and $A = 32$–40 (Ref. [8]). (The computations were performed on a VAX-780 computer over a period of about 2 years beginning in the middle of 1980.) The parameters were the 3 *sd*-shell SPE and 63 *sd*-shell TBME, and of these, 47 (out of the 66) linear combinations of parameters were varied in the last iteration.

The rms difference between the experimental and the theoretical binding energies in this 47-parameter fit was about 185 keV. Since the errors on the experimental binding energies are usually much less than 185 keV, the usual normalized χ value is very large. In order to obtain a more equitable weighting of the

experimental data as well as to obtain an estimate of the errors on the parameters, a theoretical error of 150 keV was added in quadrature to the experimental error of the majority of the data, for which the model-experimental correspondences were certain, and an additional 150-keV error was added in quadrature to some (about 15%) of the higher-lying states for which the correspondences were not unambiguous. With these additions, the normalized χ was 1.07 for the 47-parameter fit. All subsequent fits discussed here include these additional theoretical errors and the resulting χ values should be compared to the "best" value of about 1.0. The rms

TABLE II

Values of χ for the Linear Combination (LC) Fits as a Function of the Total Number of Varied Linear Combinations of Parameters (N)

	χ					
	TBME				Talmi	
N	Kuo[a]	HKT[b]	Z[c]	HKT and no ALS[d]	HKT DI[e]	HKT DD[f]
10	2.82	3.12	16.36	3.24	5.89	4.43
12	2.35	2.87	15.68	2.94	5.83	3.86
14	2.15	2.70	12.53	2.85	3.65	3.05
16	2.14	2.65	11.00	2.65	3.66	2.90
18	1.94	2.41	10.41	2.34	3.03	2.59
20	1.66	2.19	7.27	2.14	2.93	2.09
25	1.42	1.87	4.32	1.84	2.25	2.04
28					2.05	
30	1.37	1.72	3.82	1.62		1.50
32						1.40
35	1.24	1.39	3.29	1.38		
40	1.13	1.26	3.00	1.30		
45	1.08	1.18	2.80	1.28		
48				1.19		
50	1.07	1.12	1.98			
66	1.02	1.02	1.02			

Note. Fits are based on linear combinations of TBME and SPE and on linear combinations of Talmi integrals and SPE.

[a] The linear combinations of TBME not varied were set equal to the G-matrix element values of Kuo (Ref. [19]).

[b] The linear combinations of TBME not varied were set equal to the matrix elements obtained from the HKT interaction.

[c] The linear combinations of TBME not varied were set equal to zero.

[d] Same as [b] except that the 18 ALS matrix elements were constrained to be zero.

[e] The linear combinations of Talmi integrals not varied were set equal to the matrix elements obtained from the HKT interaction.

[f] Same as [e] except that the density dependence of Eq. (26) with $A_d = -1$ and $B_d = 1$ was used.

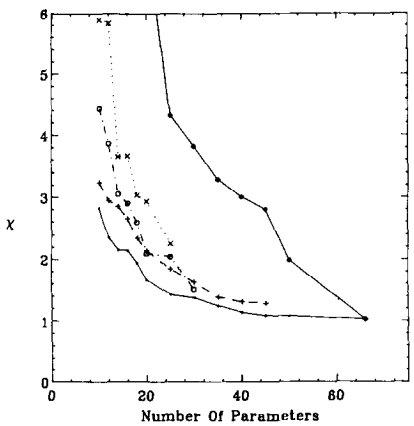

FIG. 1. Plots of the χ value obtained in various linear-combination-method fits as a function of the number of varied linear combinations of parameters. The results from Table II are: TBME-Kuo (small points connected by a solid line), TBME-Z (diamonds connected by a solid line), TBME-HKT and no-ALS (pluses connected by a dashed line), Talmi-HKT-DI (crosses connected by dots), and Talmi-HKT-DD (circles connected by a dot–dashed line).

deviation between experiment and theory in a fit where $\chi > 1$ can be estimated from the product of χ with 185 keV. The χ values for the W interaction as a function of the number of linear combinations of parameters (N) are given in column 2 of Table II and plotted in Fig. 1. The values of χ are relatively constant for $N > 45$, indicating that there are about 19 linear combinations of parameters which are poorly determined.

For completeness, we list the values of the SPE and TBME for the W interaction in Table III. Two comparisons between experimental energies and predictions of the W interaction are shown in Figs. 2 and 3. Spectra for ^{27}Al, ^{28}Si, and ^{29}Si are shown in Fig. 2. For each nucleus, the experimental excitation energies are plotted on the right-hand side and the theoretical energies obtained with the W interaction are plotted on the left-hand side, the two points being joined by a line. A horizontal line thus indicates perfect agreement between experiment and theory. The slopes of the lines are typical of the 185-keV rms deviation obtained in the least-squares fit described above. Most of the levels plotted were not included in the least-squares fit because of the large dimensions of their associated Hamiltonian matrices.

Two-neutron separation energies (Ref. [5]) are shown in Fig. 3. The values obtained with the W interaction are given by the thin solid lines connecting each chain of isotopes. The deviations between experiment and theory are indicated by the sizes of the circles. Most of the circles are small and consistent with the 185-keV rms. A few quite large deviations appear for the most neutron-rich Na and Mg isotopes. This may indicate the disappearance of the $N = 20$ shell closure for these large N/Z ratios.

TABLE III

Values of the Two-Body Matrix Elements (TBME) for Wildenthal's Model-Independent *sd*-Shell Hamiltonian

$2j_a$	$2j_b$	$2j_c$	$2j_d$	$2J$	$2T$	TBME (MeV)	$2j_a$	$2j_b$	$2j_c$	$2j_d$	$2J$	$2T$	TBME (MeV)
5	5	5	5	0	2	−2.8197	5	3	5	3	2	0	−6.5058
5	5	5	5	2	0	−1.6321	5	3	5	3	2	2	1.0334
5	5	5	5	4	2	−1.0020	5	3	5	3	4	0	−3.8253
5	5	5	5	6	0	−1.5012	5	3	5	3	4	2	−0.3248
5	5	5	5	8	2	−0.1641	5	3	5	3	6	0	−0.5377
5	5	5	5	10	0	−4.2256	5	3	5	3	6	2	0.5898
5	5	5	1	4	2	−0.8616	5	3	5	3	8	0	−4.5062
5	5	5	1	6	0	−1.2420	5	3	5	3	8	2	−1.4497
5	5	5	3	2	0	2.5435	5	3	1	1	2	0	2.1042
5	5	5	3	4	2	−0.2828	5	3	1	3	2	0	−1.7080
5	5	5	3	6	0	2.2216	5	3	1	3	2	2	0.1874
5	5	5	3	8	2	−1.2363	5	3	1	3	4	0	0.2832
5	5	1	1	0	2	−1.3247	5	3	1	3	4	2	−0.5247
5	5	1	1	2	0	−1.1756	5	3	3	3	2	0	0.5647
5	5	1	3	2	0	−1.1026	5	3	3	3	4	2	−0.6149
5	5	1	3	4	2	−0.6198	5	3	3	3	6	0	2.0337
5	5	3	3	0	2	−3.1856	1	1	1	1	0	2	−2.1246
5	5	3	3	2	0	0.7221	1	1	1	1	2	0	−3.2628
5	5	3	3	4	2	−1.6221	1	1	1	3	2	0	1.2501
5	5	3	3	6	0	1.8949	1	1	3	3	0	2	−1.0835
5	1	5	1	4	0	−1.4474	1	1	3	3	2	0	0.0275
5	1	5	1	4	2	−0.8183	1	3	1	3	2	0	−4.2930
5	1	5	1	6	0	−3.8598	1	3	1	3	2	2	0.6066
5	1	5	1	6	2	0.7626	1	3	1	3	4	0	−1.8194
5	1	5	3	4	0	−0.0968	1	3	1	3	4	2	−0.4064
5	1	5	3	4	2	−0.4770	1	3	3	3	2	0	0.3983
5	1	5	3	6	0	1.2032	1	3	3	3	4	2	−0.5154
5	1	5	3	6	2	−0.6741	3	3	3	3	0	2	−2.1845
5	1	1	3	4	0	−2.0664	3	3	3	3	2	0	−1.4151
5	1	1	3	4	2	−1.9410	3	3	3	3	4	2	−0.0665
5	1	3	3	4	2	−0.4041	3	3	3	3	6	0	−2.8842
5	1	3	3	6	0	0.1887							

Note. The TBME are mass dependent as given in Eq. (14) of the text and are given here for $A = 18$. The single-particle energies are −3.9478 MeV ($0d_{5/2}$), −3.1635 MeV ($1s_{1/2}$), and 1.6466 MeV ($0d_{3/2}$).

II.D. *The* ALS *Interaction in the* sd *Shell*

In Ref. [16] the W interaction was compared with a variety of other interactions from the point of view of the spin-tensor decomposition. We review that work here with an emphasis on the importance of the ALS component. As a basis for these comparisons, the W interaction was reformulated by fitting the 63 linearly indepen-

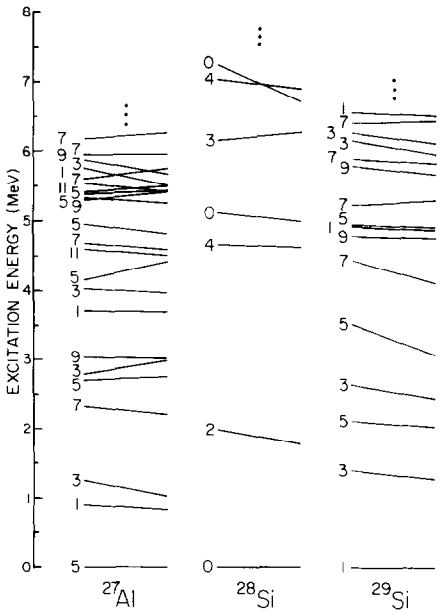

FIG. 2. Experimental (right) vs theoretical (left) energy levels calculated with the W interaction for ^{27}Al, ^{28}Si, and ^{29}Si.

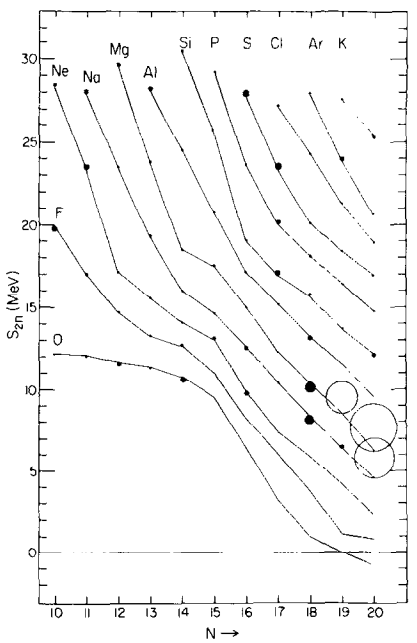

FIG. 3. Two-neutron separation energies as a function of neutron number N.

dent spin-tensor *LS*-coupled matrix elements (via the TBMECOMP of Eq. (13)) and the three single-particle energies of the *sd* shell to the 447 *sd*-shell data, with all 66 parameters varied. The resulting matrix elements and the associated diagonal uncertainties were plotted in Ref. [16], and the matrix elements are shown here in Fig. 4 (squares in the upper part of the figure). For clarity, the error bars have been suppressed. This 66-parameter interaction is essentially the same as the 47-parameter W interaction discussed in Section II.C.

The so-called antisymmetric spin–orbit (ALS) component corresponds to those *LS*-coupled matrix elements which have $S \neq S'$. The number of linearly independent matrix elements for each spin-tensor component are given in Table IV, and we see that 18 of the 63 *sd*-shell TBME are of this type. For two-nucleon scattering, antisymmetry of the two-particle wavefunction implies that $(-1)^{l+S+T} = (-1)^{l'+S'+T'}$ for the quantum numbers of the initial and final states where l is the relative angular momentum. Interactions which are parity conserving

TABLE IV

Number (N) of Independent Parameters for the Various Components of the Spin-Tensor Matrix Elements in the *sd* Shell

Type	p	S	S'	T	N	I_{DI}	I_{DD}
Central							
Singlet, odd	0	0	0	0	3	2	3
Singlet, even	0	0	0	1	7	4	5
Triplet, even	0	1	1	0	7	4	5
Triplet, odd	0	1	1	1	3	2	3
Total					20	12	16
Spin–orbit							
Even	1	1	1	0	4	3	3
Odd	1	1	1	1	5	3	3
Total					9	6	6
Tensor							
Even	2	1	1	0	10	4	4
Odd	2	1	1	1	6	3	3
Total					16	7	7
Antisymmetric Spin–orbit							
	1	0	1	0	9		
	1	0	1	1	9		
Total					18		
Total					63	25	29

Note. The number of independent Talmi integrals are also listed for the density-independent case (I_{DI}) and the density-dependent case (I_{DD}). "Singlet" and "triplet" refer to the multiplicity of $(2S+1)$ and "even" and "odd" refer to the parity of the relative l.

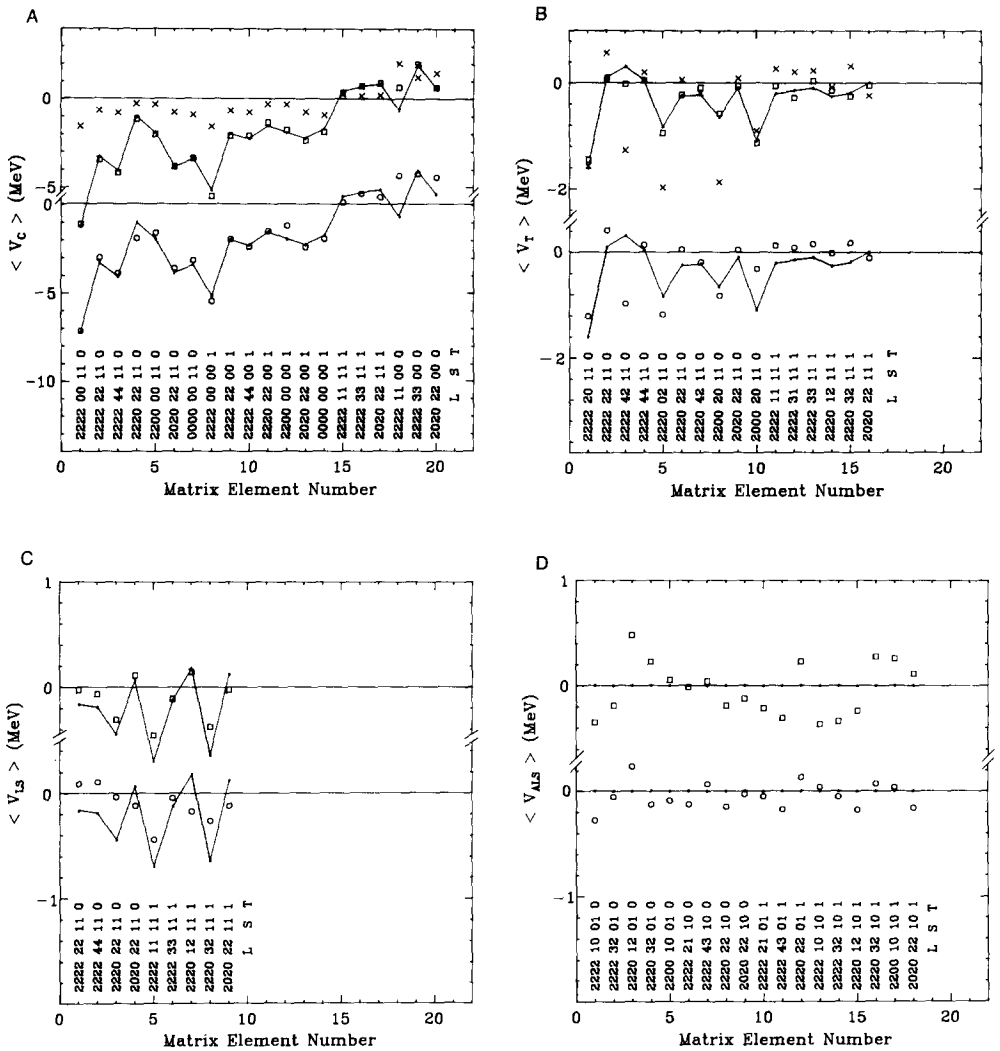

FIG. 4. (A) Matrix elements for the central component. In the top panel the 66-parameter model-independent TBME (squares) are compared to the WNOALS TBME (solid line) obtained in the 48-parameter fit when the antisymmetric spin–orbit component is constrained to be zero. In the bottom panel the WNOALS TBME are compared to the renormalized G-matrix elements of Kuo (circles). Also, in the upper panel the TBME obtained with the OPEP potential are shown (crosses). In this and other figures, the labels corresponding to the matrix element numbers along the x-axis are the quantum numbers $l_a l_b l_c l_d$ LL' SS' T in the LS-coupled matrix element $\langle l_a l_b\, LS\, JT \,|V|\, l_c l_d\, L'S'\, JT\rangle$. (B) Matrix elements for the tensor component. The same interactions as those in (A) are compared and the conventions are the same. (C) Matrix elements for the spin–orbit component. The same interactions as those in (A) are compared and the conventions are the same. (D) Matrix elements for the antisymmetric spin–orbit component. The same interactions as those in (A) are compared and the conventions are the same.

$[(-1)^l = (-1)^{l'}]$ and isospin conserving ($T = T'$) must then also conserve the total spin. Thus, for the bare G-matrix the ALS terms vanish.

Core-polarization corrections to the G-matrix give rise to nonzero but small ALS matrix elements (Refs. [16, 20]). The ALS matrix elements obtained from the renormalized G-matrix of Kuo are shown in the bottom panel of Fig. 4D; they are in fair agreement with, those obtained from the "W" interaction as shown in the top panel of Fig. 4D. Earlier studies of the empirical interaction using MI methods sometimes lead to much larger emprirical values for the ALS matrix elements (Ref. [15]), as a result of being inadequately constrained by the data. This has prompted several previous investigations into the necessity of including ALS components in the shell-model interaction (Refs. [21–23]). In Ref. [16] we found that the ALS matrix elements are small and relatively poorly determined by the MI fit to the 447 *sd*-shell data.

To obtain another measure of the importance of the ALS terms, we have repeated the least-squares fit with the 18 ALS matrix elements constrained to be zero. The χ value increases from 1.02 in the 66-parameter fit to 1.19 in the constrained "48-parameter plus no-ALS" fit. This translates into about a 25-keV increase in the rms deviation. This result can be compared to what happens when the other spin-tensor components of the interaction are similarly constrained to be zero, namely for central $= 0$, $\chi = 20.6$; for tensor $= 0$, $\chi = 1.69$; and for spin–orbit $= 0$, $\chi = 2.26$. Again, we conclude that ALS term is relatively unimportant for this selection of 447 binding-energy data.

The TBME spin-tensor components obtained from this no-ALS fit are plotted in Fig. 4 (solid lines in upper and lower parts of the figures). In the following, we will refer to the two-body matrix elements obtained from this no-ALS fit as the WNOALS interaction. One can see from Fig. 4 that the 66-parameter and WNOALS interactions are in general very similar. The biggest difference can be seen in the spin–orbit component where the WNOALS interaction is somewhat larger numerically than the 66-parameter interaction. Since all of the model-dependent interactions considered below have no ALS component, they will be compared to the WNOALS interaction.

III. Potential Models for the Effective Interaction

III.A. *General Formulation*

As our principal model for the effective interaction we assume a potential with a general form for the central (c), spin–orbit (s), and tensor (t) components as follows:

$$\begin{aligned} V_c(S, T) &= V_0(S, T) = P^{ST} D_0(R, S, T)\, d_c(r_{12}, S, T) \\ V_s(S, T) &= V_1(S, T) = P^{ST} D_1(R, S, T)\, d_s(r_{12}, S, T)\, \mathbf{L}\cdot\mathbf{S} \\ V_t(S, T) &= V_2(S, T) = P^{ST} D_2(R, S, T)\, d_t(r_{12}, S, T)\, S_{12}. \end{aligned} \tag{15}$$

In expression (15), the P^{ST} are projection operators for the four (S, T) channels (0, 0), (0, 1), (1, 0), and (1, 1), $\mathbf{S} = (\boldsymbol{\sigma}_1 + \boldsymbol{\sigma}_2)/2$ and $\mathbf{S}_{12}$ is the tensor operator

$$\mathbf{S}_{12} = 3(\boldsymbol{\sigma}_1 \cdot \mathbf{r}_{12})(\boldsymbol{\sigma}_2 \cdot \mathbf{r}_{12}) - (\boldsymbol{\sigma}_1 \cdot \boldsymbol{\sigma}_2). \tag{16}$$

The $\mathbf{r}_{12}$ and $\mathbf{R}$ are the relative and center-of-mass coordinates ($r_{12} = |\mathbf{r}_{12}|$ and $R = |\mathbf{R}|$), where

$$\mathbf{r}_{12} = \mathbf{r}_1 - \mathbf{r}_2$$

and

$$\mathbf{R} = (\mathbf{r}_1 + \mathbf{r}_2)/2. \tag{17}$$

The function $d(r_{12})$ describes the dependence of the potential on the relative coordinate, and the function $D(R)$ describes the dependence on the center-of-mass coordinate—this latter degree of freedom referring to the density dependence to be discussed in Section III.B [for a density-independent interaction $D(R) = 1$].

The interaction of Eq. (15) can be cast in the form of Eq. (10) with U and X given by

$$U^p = D_p(R, S, T)\, d^p(r_{12}, S, T), \tag{18}$$

where

$$\begin{aligned} d^0(r_{12}, S, T) &= d_c(r_{12}, S, T) \\ d^1(r_{12}, S, T) &= d_s(r_{12}, S, T)\, \mathbf{L} \\ d^2(r_{12}, S, T) &= d_t(r_{12}, S, T)\, C^{(2)} \end{aligned} \tag{19}$$

and

$$\begin{aligned} X^0 &= P^{ST} \\ X^1 &= P^{ST}\mathbf{S} \\ X^2 &= P^{ST}(6)^{1/2}[\boldsymbol{\sigma}_1 \otimes \boldsymbol{\sigma}_2)]^{(2)} \end{aligned} \tag{20}$$

and where $C^{(2)} = (4\pi/5)\, Y^{(2)}$.

We evaluate the matrix elements of these types of potentials by using harmonic-oscillator radial wavefunctions and the standard Talmi–Moshinky transformation technique. For completeness, we give here the explicit expressions for the LS-coupled matrix elements of V_p which can be used in combination with Eq. (13) to obtain the jj-coupled matrix elements. First the antisymmetric and normalized TBME are reduced to a sum of nonantisymmetric (na) direct and exchange terms:

$$\begin{aligned} &\langle ABLSJT|\, V_p\, |CDL'S'JT\rangle \\ &\quad = [(1+\delta_{AB})(1+\delta_{CD})]^{-1/2}[\langle ABLST|\, V_p\, |CDL'S'JT\rangle_{\mathrm{na}} \\ &\qquad - (-1)^{l_c + l_d - L' - S' - T}\langle ABLSJT|\, V_p\, |DCL'S'JT\rangle_{\mathrm{na}}]. \end{aligned} \tag{21}$$

With Eq. (10), these LS-coupled matrix elements are then expressed in terms of space- and spin-reduced matrix elements, e.g.,

$$\langle ABLSJT|\, V_p \,|CDL'S'JT\rangle_{\text{na}} = (-1)^{S+L'+J} \begin{Bmatrix} L & S & J \\ S' & L' & p \end{Bmatrix} \times \langle ABL\|\, U^p \,\|CDL'\rangle \langle ST\|\, X^p \,\|S'T\rangle. \tag{22}$$

Next, the spatial wavefunctions $|AB\rangle$ and $|CD\rangle$ are expressed in terms of the relative (n, λ) and center-of-mass (N, Λ) coordinates using the Talmi–Moshinsky transformation (Ref. [17]):

$$\langle ABL\|\, U^p \,\|CDL'\rangle = \sum_{n,\lambda,n',\lambda',N,\Lambda,N',\Lambda'} \langle n\lambda N\Lambda \mid ABL\rangle \langle n'\lambda' N'\Lambda' \mid CDL'\rangle \times \langle n\lambda N\Lambda L\|\, U^p \,\|n'\lambda' N'\Lambda' L'\rangle. \tag{23}$$

Finally, this last integral reduces to

$$\langle n\lambda N\Lambda L\|\, U^p \,\|n'\lambda' N'\Lambda' L'\rangle = (-1)^{\lambda+\Lambda+L+p}[(2L+1)(2L'+1)]^{1/2} \begin{Bmatrix} \lambda & \lambda' & p \\ L' & L & \Lambda \end{Bmatrix} \times \langle n\lambda\|\, d^p(r_{12}) \,\|n'\lambda'\rangle \langle N\Lambda|\, D_p(R) \,|N'\Lambda'\rangle\, \delta_{\Lambda,\Lambda'}. \tag{24}$$

In the case of density-independent potentials the center-of mass integral is just $\delta_{N,N'}$. With the $d(r_{12})$ given by Eqs. (19) the relative integrals reduce to

$$\begin{aligned} \langle n\lambda\|\, d^0(r_{12}) \,\|n'\lambda'\rangle &= \langle n\lambda|\, d_c(r_{12}) \,|n'\lambda'\rangle (2\lambda+1)^{1/2}\, \delta(\lambda, \lambda') \\ \langle n\lambda\|\, d^1(r_{12}) \,\|n'\lambda'\rangle &= \langle n\lambda|\, d_s(r_{12}) \,|n'\lambda'\rangle [\lambda(\lambda+1)(2\lambda+1)]^{1/2}\, \delta(\lambda, \lambda') \\ \langle n\lambda\|\, d^2(r_{12}) \,\|n'\lambda'\rangle &= \langle n\lambda|\, d_t(r_{12}) \,|n'\lambda'\rangle \\ &\quad \times (-1)^{\lambda}[(2\lambda+1)(2\lambda'+1)]^{1/2} \begin{Bmatrix} \lambda & 2 & \lambda' \\ 0 & 0 & 0 \end{Bmatrix}. \end{aligned} \tag{25}$$

III.B. *Density Dependence*

Phenomenological density-dependent interactions have long played an important role in Hartree–Fock calculations (see, for example, Refs. [24–26]) as well as in shell-model calculations (see, for example, Refs. [7, 27, 28]). From a more fundamental point of view, density dependence enters into the calculations of the G-matrix in finite nuclei (Ref. [29]). There also has been a renewed interest in density dependence because of recent developments with relativistic models, e.g., Ref. [30].

We introduce density dependence into our model studies with the form

$$D(R) = 1 + A_d F(R)^{B_d},$$

with

$$F(R) = \{1 + \exp[(R - R_0)/a]\}^{-1}, \tag{26}$$

where A_d and B_d are constants to be chosen. Initially we take $R_0 = 1.1A^{1/3}$ fm (with $A = 16$ for the *sd* shell) and $a = 0.6$ fm. We assume a simple linear density dependence ($B_d = 1$), as in the original Skyrme Hartree–Fock calculations (Ref. [31]) and work by Migdal (Ref. [28]). Note that $F(R)$ is the Fermi function which approaches unity as R goes to zero.

It is interesting to compare this density dependence with the commonly used surface-delta interaction (SDI) for the central component (Refs. [7, 27]). For a zero-range interaction the radial dependence of the two-body matrix element reduces to the integral (Ref. [7])

$$I = \int D(R)\, \psi_A(R)\, \psi_B(R)\, \psi_C(R)\, \psi_D(R)\, R^2\, dR. \tag{27}$$

For a surface-delta interaction, one could evaluate this integral with $D(R) = \delta(R - R_0)$ for some value of R_0 near the surface. However, in practice one usually replaces the integral by unity times a phase factor which takes into account the fact that the radial wavefunctions $\psi(R)$ conventionally are defined to be positive near the origin:

$$I = (-1)^{n_a + n_b + n_c + n_d}. \tag{28}$$

A more realistic form of the density dependence is given by $D(R)$ in Eq. (26) with $A_d = -1$ (i.e., an interaction which goes smoothly to zero in the nuclear interior). In Table V we compare the radial matrix elements for the *sd* shell calculated with a density-*in*dependent zero-range interaction and with various versions of the density-dependent, zero-range interactions. We note the very large differences obtained with the various models. Also, we note that our linear density dependence gives results which are closest to the commonly used constant approximation (Eq. (28)).

We have not made a complete study of the sensitivity of the *sd*-shell binding energy data to the A_d parameter. However, the results of a limited search over values of A_d with our "best-fit" interaction (see Section IV.D) gave a minimum χ for $A_d = -1$. For the remaining discussion concerning density dependence (Section IV) we thus confine our attention to the "surface interaction" obtained by using $A_d = -1$ in Eq. (26). Many of the successful phenomonological global interactions, such as the D1 interaction of Decharge and Gogny (Ref. [25]), have a density dependence which makes the interaction much smaller in the nuclear interior than on the surface.

III.C. *Representation in Terms of Talmi Integrals*

The relative-coordinate harmonic-oscillator radial matrix elements in Eq. (24) can be simply evaluated numerically. However, some insight can be gained by expanding these matrix elements in terms of Talmi integrals (Ref. [32]),

$$\langle n\lambda |\, d(r)\, | n'\lambda' \rangle = \sum_q B_q(n, \lambda, n', \lambda')\, I_q, \tag{29}$$

TABLE V

Comparison of *sd*-Shell Radial Matrix Elements Calculated with Zero-Range Density-Dependent and Density-Independent Interactions

				I			
A	B	C	D	DI[a]	DD[b]	SDI1[c]	SDI2[d]
				Absolute values			
$0d$	$0d$	$0d$	$0d$	0.0411	0.0207		
				Values relative to $0d$–$0d$–$0d$–$0d$			
$0d$	$0d$	$0d$	$0d$	1.000	1.000	1.000	1.000
$0d$	$0d$	$0d$	$1s$	−0.527	−0.725	−0.685	−1.000
$0d$	$0d$	$1s$	$1s$	0.595	0.672	0.462	1.000
$0d$	$1s$	$1s$	$1s$	−0.113	−0.564	−0.322	−1.000
$1s$	$1s$	$1s$	$1s$	2.440	0.754	0.220	1.000

Note. The values are compared relative to the $0d$ matrix element. Harmonic-oscillator radial wavefunctions were used with $b = 1.721$ fm for the length parameter.

[a] The density-independent interaction obtained with $D(R) = 1$ in Eq. (26).

[b] The density-dependent interaction obtained with $D(R)$ given by $A_d = -1$ and $B_d = 1$ in Eq. (26).

[c] The density-dependent interaction obtained with $D(R)$ given by $\delta(R - R_0)$, with $R_0 = 1.1\ (16)^{1/3}$.

[d] The density-dependent interaction obtained with the constant radial-integral approximation of Eq. (28).

where

$$I_q = [2/\Gamma(q + 3/2)] \int r^{2q} \exp(-r^2)\, d(r)\, r^2\, dr. \tag{30}$$

The index q runs from a minimum value of $(\lambda + \lambda')/2$ to a maximum value of $n + n' + (\lambda + \lambda')/2$. The B coefficients can be calculated analytically (Ref. [32]).

The above expansion is particularly useful when no radial dependence of the two-particle interaction has been postulated, since then the Talmi integrals I_q may be left as parameters in the fit, to be adjusted by comparison with the appropriate experimental data. It is especially important to realize that the range of allowed values of q puts a strict upper limit on the number of parameters which can be determined within the framework of potential models.

The short-range behavior of the interaction has the strongest effect on the Talmi integrals of lower order q. In the case of a delta interaction, I_0 will be the only non-vanishing integral. The number of independent Talmi integrals for each component of the interaction are listed in Table IV. In addition to the minimum and maximum ranges on q mentioned above (e.g., $q = 0$ to 4 for the *sd* shell) there are other considerations which further limit the number of nonvanishing terms. The most

obvious of these is that the $q=0$ (delta-function) term cannot contribute to the $(S, T)=(0, 0)$ and $(1, 1)$ channels of the central component or to the spin–orbit or tensor components. From an examination of the linear dependence of the various terms, we find a total of 25 independent Talmi integrals for density-independent potentials. If the potential is density dependent this number goes up to 29.

III.D. *Parameterizations of the Potential*

A large variety of specific potential-model parameterizations has been proposed and discussed in the literature. In this section we examine a few of these in comparison with the W interaction of the *sd* shell. The purpose is to determine which, if any, of these can be used as guidance or a starting point for our *sd*-shell fits and for subsequent work of this type. Two classes of interactions will be discussed: phenomonological parameterizations based on fits to global nuclear properties such as the binding energies and radii of closed-shell nuclei and microscopic parameterizations based on fits to G-matrix elements derived from nucleon–nucleon scattering data.

In the first class we consider the central components of three interactions. The TBME obtained from these are compared in Fig. 5 with the WNOALS interaction.

(1) The Schiffer–True interaction (Ref. [33]) pluses in the figure). Two Yukawa-type potentials ($r_1=1.415$ fm and $r_2=2.0$ fm) are taken for each of the four central channels. The eight parameters were obtained from a fit to the diagonal TBME obtained from a wide variety of nuclei which are two particles or two holes

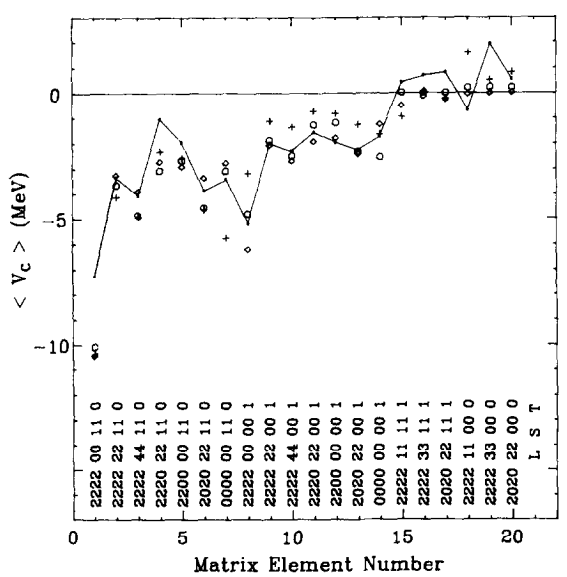

FIG. 5. Matrix elements for the central component. The WNOALS TBME are compared to those obtained from the Schiffer–True interaction (pluses) the SGII interaction (diamonds), and the DI interaction (circles). See Section III.D of the text.

removed from the closed-shell nuclei. The TBME were evaluated with harmonic-oscillator radial wavefunctions with $\hbar\omega = 14$ MeV.

(2) The SGII interaction of van Giai and Sagawa (Ref. [24]) (diamonds in the figure). This is an eight-parameter density-dependent Skyrme-type interaction. The parameters were obtained from a fit to binding energies, sizes, and excitation energies of giant resonances in the closed-shell nuclei. In addition, in contrast to most other Skyrme-type parameterizations, the average attractive pairing properties of the $T = 1$ interaction were considered. The TBME shown in the figure were obtained from the work of Ref. [34], where Hartree–Fock radial wavefunctions were used.

(3) The D1 interaction of Decharge and Gogny (Ref. [25]) (circles in the figure). Potentials of the two-Gaussian type are taken for each of the four central channels plus a two-parameter density-dependent delta function. The 10 parameters were determined from a fit to a variety of global properties of closed-shell nuclei. The TBME shown in the figure were evaluated with harmonic-oscillator radial wavefunctions with $\hbar\omega = 14$ MeV.

All three of these interactions agree qualitatively with the *sd*-shell WNOALS interaction (the solid line in Fig. 5). However, on a quantitative level the agreement is poor, and they could not compete with the WNOALS interaction in terms of the quality of the spectra unless the parameters could be modified.

The second class of potential parameterizations we consider are those based on nucleon–nucleon scattering data. In particular we consider those obtained with the method of Bertsch *et al.* (Ref. [35]) and subsequently revised and updated by Anantaraman *et al.* (Ref. [36]) and Hosaka *et al.* (Ref. [6]). This method consists of first calculating (with some approximations) the Brueckner bare G-matrix elements in finite nuclei from some established form of the realistic nucleon–nucleon (N–N) interaction determined from scattering data. These G-matrix elements are then fitted to some assumed form for $d(r)$ in Eq. (15). We note that any explicit density dependence is averaged out and removed in the approximation used in Ref. [6] to calculate the G-matrix elements.

In Fig. 6 we compare the WNOALS interaction with the TBME obtained from several of these G-matrix-type potentials and with the original bare G-matrix of Kuo (Ref. [19]). In the figure are shown the TBME derived from the following.

(1) The original bare G-matrix elements of Kuo (crosses in the upper part of the figure). These are based on the Hamada–Johnston N–N interaction.

(2) The four-Yukawa potential fitted to G-matrix elements based on the Reid soft-core N–N interaction (Ref. [36]) (squares in the upper part of the figure).

(3) The four-Yukawa potential fitted to G-matrix elements based on the Paris N–N interaction (Ref. [36]) (circles in the lower part of the figure).

(4) The one-boson-exchange potential type fitted to G-matrix elements based on the Paris N–N interaction (Ref. [6]) (pluses in the lower part of the figure).

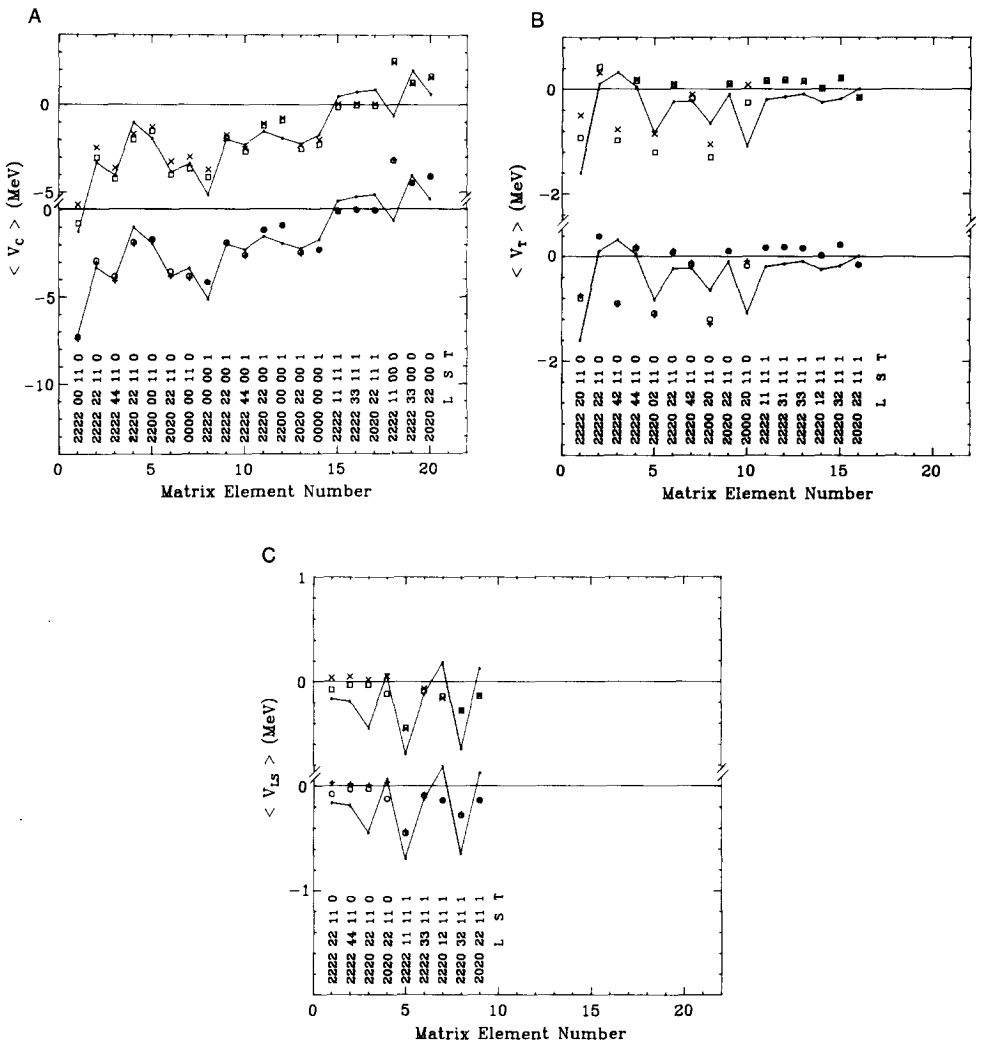

FIG. 6. (A) Matrix elements for the central component. In the top panel the WNOALS TBME are compared with the bare G-matrix values of Kuo (crosses) and Anantaraman *et al.* (Paris potential, squares). In the bottom panel the WNOALS TBME are compared with the bare G-matrix values of Anantaraman *et al.* (Reid potential, circles) and Hosaka *et al.* (Paris potential, pluses). (B) Matrix elements for the tensor component. The same interactions as those in (A) are compared and the conventions are the same. (C) Matrix elements for the spin–orbit component. The same interactions as those in (A) are compared and the conventions are the same.

It is immediately apparent that all four of these interactions give nearly identical values for the TBME for all three components. If the central component of the Kuo G-matrix is scaled up in magnitude by about 10% it would be very close to the other three results for the central interaction. Another observation is that the bare G-matrix is already quite close to the WNOALS interaction. The agreement is generally better than that for the phenomenological potentials discussed above.

Next we consider core-polarization corrections to the bare G-matrix which gives the renormalized G-matrix (Ref. [1]). The original renormalized G-matrix of Kuo (Ref. [19]) is compared with the WNOALS interaction in the bottom panel of Fig. 4. Overall the agreement is good. However, there is a relatively small change from the bare G-matrix (top panel of Fig. 6), and this change is sometimes but not always in the right direction to improve the agreement. In Ref. [16] we compared the WNOALS interaction with the more recent core-polarization calculations of Shurpin *et al.* (Ref. [2]). As noted in Ref. [16], even though the core-polarization calculations of Shurpin *et al.* are much more sophisticated than the original calculations of Kuo, the agreement with the W interaction appears to be significantly worse.

We do not include microscopic core-polarization corrections in the analyses of Section IV for the following reasons. (1) Microscopic calculations require extensive computational time, which makes them impractical to incorporate routinely. (2) Many assumptions and approximations go into the calculations. (3) As noted above, existing microscopic calculations do not seem to significantly improve the agreement compared to the bare G-matrix. (4) One might hope that the core-polarization corrections lead to modifications which can be accounted for phenomenologically by modification of the interaction strengths, and/or modification of the density dependence, and/or addition of multipole terms (Section III.F).

For the starting point of our potential-model parameterizations we have chosen to use the bare G-matrix of Hosaka, Kubo, and Toki (Ref. [6]) which will be referred to as the HKT interaction. Details of the HKT interaction are discussed in the next section.

III.E. *The* HKT *Interaction*

Hosaka, Kubo, and Toki (Ref. [6]) parameterized their bare G-matrix in terms of the standard one-boson-exchange potential (OBEP) forms (Ref. [37]) for $d(r_{12})$, given by

$$
\begin{aligned}
d_c(r_{12}, S, T) &= \sum_i \mathrm{SP}_c(i, S, T) \exp(-x_i)/x_i \\
d_s(r_{12}, S, T) &= \sum_i \mathrm{SP}_s(i, S, T)[1 + (1/x_i)] \exp(-x_i)/x_i^2 \\
d_t(r_{12}, S, T) &= \sum \mathrm{SP}_t(i, S, T)[1 + (3/x_i) + (3/x_i^2)] \exp(-x_i)/x_i,
\end{aligned}
\tag{31}
$$

where x_i is r_{12} divided by the interaction range μ_i. The HKT parameterization requires four ranges for the central component: $\mu = 0.20$, 0.33, 0.50, and 1.414 fm; two ranges for the tensor component: $\mu = 0.25$ and 1.414 fm; and two ranges for the spin–orbit component: $\mu = 0.25$ and 0.40 fm.

The strength parameters SP were obtained from a fit to G-matrix elements calculated from the Paris N–N potential (Ref. [38]) and are given in Ref. [6, Table 2]. Within the approximations of Ref. [6], the density-dependent term $D(R)$ is unity for all channels.

The longest ranged part of the HKT interaction corresponds to the standard one-pion-exchange potential (OPEP). The standard OPEP interaction is shown in the top panels of in Fig. 4 (crosses). The OPEP contribution to the bare G-matrix is seen to provide about one-third of the attractive interaction needed for the $(S, T) = (0, 1)$ and $(1, 0)$ channels of the central component.

A common feature of this as well as other OBEP parameterizations is a strong attractive medium-range part which is cancelled out by a strong repulsive short-range part. For example, for the HKT interaction, the total value for the diagonal $(d_{5/2})^2$ $J=0$, $T=1$ matrix element of -1.542 MeV can be decomposed into 11.712 MeV [$(S, T) = (0, 1)$ central, $\mu = 0.20$], -13.253 MeV [$(S, T) = (0, 1)$ central, $\mu = 0.33$ plus $\mu = 0.50$], -0.964 MeV [$(S, T) = (0, 1)$ central, $\mu = 1.414$], -0.041 MeV [$(S, T) = (1, 1)$ central, all ranges], 0.324 MeV [total tensor], and 0.680 MeV [total spin–orbit]. Although both the short- and the medium-range terms give rise to similar, delta-function type behaviors for the TBME, the large cancellation in the sum can give a total which is qualitatively different. This is not so important for the *sd*-shell matrix elements, but for the high-spin orbits in heavier nuclei this cancellation gives rise to an "antipairing" effect in the bare G-matrix elements (i.e., the result that the $J=2$, $T=1$ matrix element is sometimes more attractive than the $J=0$, $T=1$ matrix element) (Ref. [39]).

III.F. *Multipole Interactions*

We include multipole interactions in our analysis because they can be easily calculated without the complex formalism of Section III.A and because they have played an important role in earlier effective interaction analyses. For the central component we assume

$$V_c^M(S, T) = \sum_{S,T} \left[P^{ST} C_0(S, T) + \sum_{L>0}^{L_{\max}} P^{ST} C_L(L, S, T)\, M^{(L)}(\mathbf{r}_1) \cdot M^{(L)}(\mathbf{r}_2) \right], \quad (32)$$

where C_L are strength parameters to be determined and the simple monopole term ($L=0$) is separated from the higher multipoles. The one-body multipole operator, $M^{[L]}$, is given by

$$M^{(L)}(\mathbf{r}) = f_L(r)\, Y^{(L)}(\mathbf{r}). \quad (33)$$

The $f_L(r)$ are radial form factors, commonly taken to be just r^L, but more

realistically taken to be proportional to the Tassie model transition density (Ref. [40]) for the mean-field potential $V^a(r)$,

$$f_L(r) = r^{L-1} d[V(r)/V(r=0)]/dr. \tag{34}$$

For $V(r)$ we assume the usual Saxon–Woods form

$$V(r) = V_v\{1 + \exp[(r - R_v)/a_v]\}^{-1}.$$

We take $R_v = 1.2A^{1/3}$ (with $A = 16$ for the sd shell) and $a_v = 0.7$. (In the numerical calculations an overall L-dependent normalization of 50 $(R_v)^L$ is introduced so that the matrix elements of interest are on the order of unity.)

The core-polarization contribution to the interaction is often parameterized in terms of these multipole interactions (Refs. [41, 42]). Many schematic interactions often include only the $L = 2$ quadrupole term. However, we note that higher L terms are also important in microscopic core-polarization calculations (Refs. [41, 42, 39]). The value of $L_{\max}$ is given by two times the highest l value for the single-particle orbits in the model space; e.g., $L_{\max} = 4$ for the sd shell. The values of L are also limited by the parity of the model-space orbits; for the sd shell only even values of L are permitted.

We have found that the central components of the sum of the core-polarization terms G_{3p1h}, G_{2p}, and G_{2h} calculated by Kuo (Ref. [19]) can be well described in terms of V_c^M with three terms ($L = 0$, 2, and 4) for each of the four (S, T) channels. [Of course, this is nontrivial only for the $(S, T) = (0, 1)$ and $(1, 0)$ channels; for the $(S, T) = (0, 0)$ and $(1, 1)$ channels there can be at most only three independent matrix elements; see Table IV.]

It is possible to write down schematic multipole interactions for the spin–orbit and tensor terms which are analogous to Eq. (32),

$$V_s^M \propto [M^{(L)}(\mathbf{r}_1) \otimes M^{(L)}(\mathbf{r}_2)]^{(1)} \cdot [\boldsymbol{\sigma}_1 \otimes \boldsymbol{\sigma}_2]^{(1)}$$

for the spin–orbit component and

$$V_t^M \propto [M^{(L)}(\mathbf{r}_1) \otimes M^{(L)}(\mathbf{r}_2)]^{(2)} \cdot [\boldsymbol{\sigma}_1 \otimes \boldsymbol{\sigma}_2]^{(2)}$$

for the tensor component.

V_s^M contributes to the antisymmetric spin–orbit (ALS) component and vanishes for the spin–orbit component. Core-polarization corrections do give rise to non-vanishing ALS matrix elements (Refs. [16, 20]), and we have had some success in using V_s^M to mock up the ALS component of the renormalized Kuo interaction. However, we find that only about one-half of the additional rms deviation of 25 keV mentioned in Section II.C can be accounted for by this schematic interaction with four parameters ($L = 2$ and 4 for the $(S, S', T) = (0, 1, 1)$ and $(0, 1, 0)$ channels). We feel that this 12 keV increase in the rms deviation value costs too much in terms of introducing a complicated and poorly understood component of

the interaction and hence omit it. In addition, V_t^M does not seem to be important for improving the fit to the tensor components of the interaction, and we do not include this term in the present analysis either.

IV. Results

In this section we discuss the results obtained for a variety of least-squares fits to the *sd*-shell binding-energy data. We emphasize that we are fitting directly to the original data set of 447 binding energies considered in Ref. [5] rather than indirectly to the set of 63 *jj*-coupled matrix elements obtained from the MI fit discussed in Section II.C. This is important because of correlations in the data set which may not be reflected in the 63 TBME of the W interaction. In the following discussion many abbreviations are used and for convenience these are summarized in Table VI.

First we list the basic assumptions (see Section II.C for more details about the first five):

(1) The wavefunctions have good isospin.

(2) The TBME used for the values of the poorly determined linear combinations in the fit were those obtained from the HKT interaction described in Section III.E.

(3) The TBME have a simple mass dependence given by Eq. (14). (This condition is relaxed in Section IV.D.)

(4) The SPE are mass independent. (This condition is relaxed in Section IV.D.)

(5) The experimental data set consists of the binding energies for 447 ground and excited states of *sd*-shell nuclei. The errors in the binding energies were taken to be the experimental value folded in quadratically with a theoretical uncertainty (see Section II.C).

(6) The OBTD and TBTD were calculated from the same set of wavefunctions as those used to obtain the W interaction discussed in Section II.C.

It would be much too time-consuming to calculate the TBTD needed for the self-consistent iteration procedure. However, these "zeroth-order" fits should be adequate, especially for those interactions of interest which are close to the W interaction. We speculate that iterations leading to a self-consistent interaction, if carried out, would result in a χ value which is slightly smaller than that obtained from the "zeroth-order" present fits.

(7) The antisymmetric spin–orbit component was taken to be zero (see Section II.D).

(8) The potential matrix elements were calculated with harmonic-oscillator radial wavefunctions with $\hbar\omega = 14$ MeV.

TABLE VI

Summary of the Symbols Used in the Text and in Other Tables

ALS	Antisymmetric spin–orbit.
C2	A fit which includes the two-parameter (one for each T value) monopole term for the central component.
C4	A fit which includes the four-parameter (one for each combination of S and T values) monopole term for the central component.
C	Either C2 or C4 as indicated by the heading.
DD	Fits in which the matrix elements of the potentials are density dependent with the density dependence given by Eq. (26) with $A_d = -1$ and $B_d = 1$.
DI	Fits in which the matrix elements of the potentials are assumed to be density independent.
FHS	A fit in which the strengths of the short-ranged OBEP terms are held fixed at the HKT interaction values.
FHSM	A fit in which the strengths of the short- and medium-ranged OBEP terms are held fixed at the HKT interaction values (see HSMn below).
FOPEP	A fit in which the strengths of the long-ranged OBEP term for the central or tensor components are held fixed at the one-pion-exchange potential values. The OPEP potential was always taken to be density independent.
H4	A fit which includes the four-parameter (one for each combination of S and T values) hexadecapole term for the central component.
HKT	The interaction obtained from a one-boson-exchange potential with the strengths of the terms given by Hosaka, Kubo, and Toki (Ref. [6]), based on a fit to G-matrix elements calculated with the Paris potential.
HSMn	A fit which includes the sum of the n short- plus medium-ranged OBEP terms (one for each combination of S and T values) with the relative strengths fixed from the HKT interaction. For the central component the OBEP terms for the three ranges $\mu = 0.20$, 0.33, and 0.50 fm were summed, and for the spin–orbit component the OBEP terms for the two ranges $\mu = 0.25$ and 0.40 fm were summed.
LC	A fit in which linear combinations of parameters are varied.
Ln	A fit which includes the n long-ranged OBEP terms (one for each combination of S and T values) with a range of $\mu = 1.414$ fm for the central ($n = 4$) and tensor ($n = 2$) components.
MI	A model-independent fit in which all possible parameters of the entire interaction or of a specified component were varied.
Mn	A fit which includes the n medium-ranged OBEP terms (one for each combination of S and T values) with ranges of $\mu = 0.50$, and 0.40 fm for the central ($n = 4$) and spin–orbit ($n = 2$) components, respectively.
OBTD	One-body transition density.
Q4	A fit which includes the four-parameter (one for each combination of S and T values) quadrupole term for the central component.
Sn	A fit which includes the n short-ranged OBEP terms (one for each combination of S and T values) with ranges of $\mu = 0.20$, 0.25, and 0.25 fm for the central ($n = 4$), tensor ($n = 2$), and spin–orbit ($n = 2$) components, respectively.
SPE	Single-particle energy.
TBME	Two-body matrix element.
TBTD	Two-body transition density.
WNOALS	The TBME obtained from the model-independent fit with the antisymmetric spin–orbit component constrained to be zero.
Z	All parameters of the specified component were constrained to be zero.

The harmonic oscillator potential was chosen in order to make use of the Talmi–Moshinsky transformation. We believe that this is an adequate approximation to more realistic radial wavefunctions. The harmonic oscillator differs from the more realistic case mostly in the lower part of the shell where the one-nucleon separation energies are the smallest. However, there is no indication in the fit to the 447 data that the average 185-keV deviation is any larger in the lower part of the $A = 16$–40 region than it is anywhere else.

(9) The density dependence, when considered, is of the form of Eq. (26) with $A_d = -1$ and $B_d = 1$. (This condition is relaxed in Section IV.D.)

TABLE VII

Results for the Fits of the Talmi Integrals

		$\chi(N)$			
Component	Terms varied	Z^b		HKT[c]	
Central	I_0	5.48	(2)	8.76	(2)
	I_0, I_1	2.33	(3)	2.60	(6)
	I_0, I_1, I_2	1.85	(10)	1.87	(10)
	I_0, I_1, I_2, I_3	1.69	(12)	1.69	(12)
	$I_0, C2$	3.80	(4)	2.24	(4)
	$I_0, C4$	3.32	(6)	1.99	(6)
	$I_0, I_1, C2$	1.73	(8)	2.01	(8)
	$I_0, I_1, C4$	1.70	(10)	1.95	(10)
Tensor	I_1	1.30	(2)	1.76	(2)
	I_1, I_2	1.25	(4)	1.30	(4)
	I_1, I_2, I_3	1.25	(6)	1.27	(6)
	I_1, I_2, I_3, I_4	1.25	(7)	1.25	(7)
Spin orbit	I_1	1.87	(1)	1.86	(1)
	I_1, I_2	1.38	(3)	1.40	(3)
	I_1, I_2, I_3	1.28	(5)	1.28	(5)
	I_1, I_2, I_3, I_4	1.24	(6)	1.24	(6)

Note. The χ value is given for each fit with the number of parameters varied (N) given in brackets.[a] See Table VI for an explanation of the symbols.

[a] The total number of model-independent terms is 20 for the central component, 16 for the tensor component, and 9 for the spin–orbit component. The results for the central component (N parameters) were obtained by allowing all tensor and spin–orbit components to vary; the total number of parameters is $N + 16 + 9 + 3$ (three for the single-particle energies). The tensor and spin–orbit components were treated in a similar manner, with the total number of parameters being $20 + N + 9 + 3$ and $20 + 16 + N + 3$, respectively.

[b] The remaining Talmi integrals of the component under consideration are set to zero.

[c] The remaining Talmi integrals are fixed to the HKT interaction values.

In this section we break the comparisons down into three main categories: Section IV.A and Tables II and VII, the results obtained from "model-independent" methods; Section IV.B and Table VIII, the results obtained from "simple" potential models; and Section IV.C and Tables IX, X, and XI, the results obtained from the more complete potential models. The main results, which include the full density-dependent OBEP potential combined with multipole terms, are included in Section IV.C. Finally, in Section IV.D we select a "best-bit" interaction and examine some of the remaining assumptions, including the assumed mass dependencies of the SPE and TBME.

The potential-model results of Sections IV.B and IV.C are presented in a number of tables which give for each type of fit the χ value along with the number of varied parameters. In most cases we investigate one component (central, spin–orbit, or tensor) of the interaction at a time. In order to obtain the most unbiased test of that particular component, model-independent (MI) forms were used for the other two components. For example, when the central component is being investigated, MI forms are used for the spin–orbit and tensor components. This was accomplished by using the TBMECOMP based on Eq. (7) for the particular potential model of the component under investigation together with TBMECOMP given by Eq. (13) for the other two components.

TABLE VIII

Results for Fits of the Strengths of Simple Central Interactions (Delta, Surface-Delta, and Monopole)

Type of central interaction and varied parameters	$\chi(N)$		
	HKT[a]	Z[b]	MI[c]
MI	3.39 (20)	3.10 (20)	1.19 (20)
δ[d]	9.29 (2)	8.21 (2)	5.48 (2)
δ, C2	5.65 (4)	5.75 (4)	3.80 (4)
δ, C4	5.45 (6)	5.35 (6)	3.32 (6)
SDI[e]	7.86 (2)	7.06 (2)	4.85 (2)
SDI, C2	5.09 (4)	2.58 (4)	2.58 (4)
SDI, C4	4.90 (6)	4.29 (6)	1.92 (6)

Note. The χ value is given for each fit, with the number of central parameters (N) given in brackets. See Table VI for an explanation of the symbols.

[a] The tensor and spin–orbit components are fixed to the HKT interaction values. The total number of parameters is $N + 3$ (three for the single-particle energies).

[b] The tensor and spin–orbit components are set to zero. The total number of parameters is $N + 3$.

[c] Model-independent forms were allowed for the tensor (16-parameter) and spin–orbit (9-parameter) components; the total number of parameters in this case is $N + 16 + 9 + 3$.

[d] The two-parameter delta interaction.

[e] The two-parameter surface-delta interaction.

TABLE IX

Results for the Fits to the Central Component

Type of interaction and varied parameters	$\chi(N)$			
Results for the model-independent (MI) method, and with all central terms constrained to be zero (Z)				
MI	1.19	(20)		
Z	20.64	(0)		
Reults for multipole interactions				
C4	6.84	(4)		
C4, Q4	3.14	(8)		
C4, Q4, H4	1.45	(12)		
Results for OBEP potentials	DI		DD	
S4	4.18	(4)	3.90	(4)
M4	3.25	(4)	3.22	(4)
L4	2.75	(4)	2.07	(4)
S4, M4	2.01	(8)	2.29	(8)
M4, L4	2.38	(8)	1.78	(8)
S4, L4	2.42	(8)	1.81	(8)
S4, M4, L4	1.82	(12)	1.35	(12)
Results for OBEP potentials with some strengths fixed at the HKT and OPEP interaction values	DI		DD	
S4, FOPEP	3.51	(4)	2.99	(4)
M4, FOPEP	2.91	(4)	2.50	(4)
S4, M4, FOPEP	2.09	(8)	1.80	(4)
FOPEP, FHSM	12.05	(0)	8.25	(0)
L4, FHSM	2.62	(4)	2.29	(4)
HSM4	2.99	(4)	2.76	(4)
HSM4, L4	2.20	(8)	1.61	(8)
Results for OBEP potentials combined with monopole terms	DI, C4		DD, C4	DD, C2
C, S4	3.05	(8)	1.68 (8)	2.27 (6)
C, M4	2.62	(8)	1.56 (8)	1.98 (6)
C, L4	2.30	(8)	1.60 (8)	1.75 (6)
C, S4, M4	1.81	(12)	1.41 (12)	1.44 (10)
C, M4, L4	1.86	(12)	1.40 (12)	1.43 (10)
C, S4, L4	1.92	(12)	1.40 (12)	1.41 (10)

Table continued

TABLE IX (*continued*)

	DI, C4		DD, C4		DD, C2	
Results for OBEP potentials with some strengths fixed at the HKT and OPEP interaction values and combined with monopole terms						
C, S4, FOPEP	2.80	(8)	1.42	(8)	1.77	(6)
C, M4, FOPEP	2.50	(8)	1.42	(8)	1.60	(6)
C, S4, M4, FOPEP	1.86	(12)	1.32	(12)	1.32	(10)
C, FHSM, FOPEP	2.62	(4)	2.78	(4)	3.90	(2)
C, L4, FHSM	2.12	(8)	1.80	(8)	1.95	(6)
C, HSM4,	2.76	(8)	2.18	(8)	2.42	(6)
C, HSM4, L4	1.90	(12)	1.36	(12)	1.41	(10)
Results for OBEP potentials with strengths fixed at the HKT and OPEP interaction values and combined with multipole terms						
C, HSM4, FOPEP	2.43	(8)	1.79	(8)	1.91	(6)
C, HSM4, Q4, FOPEP	1.70	(12)	1.68	(12)	1.75	(10)
C, HSM4, Q4, H4, FOPEP	1.34	(14)	1.36	(14)	1.36	(14)
C, FHSM, FOPEP	2.62	(4)	2.78	(4)	3.90	(2)
C, Q4, FHSM, FOPEP	2.21	(8)	1.91	(8)	2.19	(6)
C, Q4, H4, FHSM, FOPEP	1.50	(12)	1.39	(12)	1.50	(10)

Note. The χ value is given for each fit with the number of parameters (N) for the central interaction given in brackets.[a] See Table VI for an explanation of the symbols.

[a] The total number of model-independent terms is 20 for the central component, 16 for the tensor component, and 9 for the spin–orbit component. The results for the central component (N parameters) were obtained by allowing all tensor and spin–orbit components to vary; the total number of parameters is $N+16+9+3$ (three for the single-particle energies).

IV.A. *Model-Independent Results*

In Table II and Fig. 1 results of the linear combination (LC) method applied to the TBME are shown for a number of interactions and/or parameterizations frequently used in this paper. In each case the number of uncorrelated linear combinations of parameters varied for a particular interaction is plotted against the χ value of the fit to the same 447 data; the remaining poorly determined linear combinations of TBME are held fixed at some assumed values or at zero. The lowest curve in Fig. 1 (points connected by solid lines) corresponds to the case where the poorly determined combinations are fixed at the values of the renormalized Kuo interaction (Ref. [19]). Setting the poorly determined combinations equal to zero dramatically increases the χ value, as can be seen from the uppermost curve in the figure. This emphasizes the importance of the choice of interaction for the fixed combinations.

TABLE X

Results for the Fits to the Tensor Component

Type of interaction and varied parameters	$\chi(N)$	
Results for the model-independent (MI) method, and with all tensor terms constrained to be zero (Z)		
MI	1.19 (16)	
Z	1.69 (0)	
Results for OBEP potentials		
	DI	DD
S2	1.36 (2)	1.38 (2)
L2	1.49 (2)	1.48 (2)
S2, L2	1.30 (4)	1.24 (4)
Results for OBEP potentials with some strengths fixed at the HKT and OPEP interaction values		
	DI	DD
S2, FOPEP	1.82 (2)	1.77 (2)
FHS, FOPEP	2.24 (0)	2.53 (0)

Note. The χ value is given for each fit with the number of parameters (N) for the tensor interaction given in brackets.[a] See Table VI for an explanation of the symbols.

[a] The total number of model-independent terms is 20 for the central component, 16 for the tensor component, and 9 for the spin–orbit component. The results for the tensor component (N parameters) were obtained by allowing all central and spin–orbit components to vary; the total number of parameters is $20+N+9+3$ (three for the single-particle energies).

Using the HKT interaction values for the poorly determined linear combinations, the χ values, Table II, give a curve (not shown in the figure) which is only slightly above the lowest curve obtained with the Kuo interaction. The HKT bare G-matrix of course has a zero ALS component, but the values of the 18 ALS TBME may come out to be nonzero in the general LC fit. Alternatively, we can choose to fix these 18 ALS TBME matrix elements to be zero, leaving a total of 48 free parameters (fifth column of Table II). The results plotted in Fig. 1 (pluses connected by a dashed line) are again only slightly above the lowest curve.

The χ values obtained from the LC method applied to the Talmi integrals are also given in Table II and Fig. 1. Two results are shown, one for no density dependence, $D(R)=1$ (crosses connected by dots), and one for an assumed density dependence of the form of Eq. (26) (circles connected by a dot–dashed line). In both cases the poorly determined linear combinations of Talmi integrals were fixed at the HKT interaction values. The density-dependent case gives consistently lower

TABLE XI

Results for the Fits to the Spin–Orbit Component

Type of interaction and varied parameters	$\chi(N)$	
Results for the model-independent (MI) method, and with all spin–orbit terms constrained to be zero (Z)		
MI	1.19 (9)	
Z	2.26 (0)	
Results for OBEP potentials		
	DI	DD
S2	1.83 (2)	1.41 (2)
M2	1.84 (2)	1.42 (2)
S2, M2	1.73 (4)	1.38 (4)
Results for OBEP potentials with some strengths fixed at the HKT interaction values		
	DI	DD
HSM2	1.87 (2)	1.43 (2)
FHSM	1.92 (0)	2.01 (0)

Note. The χ value is given for each fit with the number of parameters (N) for the spin–orbit interaction given in brackets.[a] See Table VI for an explanation of the symbols.

[a] The total number of model-independent terms is 20 for the central component, 16 for the tensor component, and 9 for the spin–orbit component. The results for the spin–orbit component (N parameters) were obtained by allowing all central and tensor components to vary; the total number of parameters is $20 + 16 + N + 3$ (three for the single-particle energies).

χ values for the same number of parameters varied. The density-dependent Talmi-integral results are also seen to be very close to the TBME no-ALS results.

Results obtained by fitting combinations of Talmi integrals to the same basic data set are given in Table VII. While each spin-tensor component is investigated, the other two components are allowed to vary model independently. For the component under consideration, those Talmi integrals not varied are either set equal to zero (Z) or held fixed at the HKT interaction values (HKT). For the fits in Table VII we assumed no density dependence, $D(R) = 1$. The effect of adding monopole terms (C2 or C4) is also shown. The number of parameters varied reflects the restrictions on the Talmi integrals in the various (S, T) channels, referred to Section III.C.

In order to compare the Talmi-integral results of Table VII with those obtained from the potential-model parameterizations, we refer ahead to Section IV.C for Tables IX, X, and XI, in which the central, tensor, and spin–orbit components,

respectively, are treated. The Talmi-integral fits should be compared with the density-independent results of Tables IX to XI. We see that for the central component, the best χ values obtained by varying the Talmi integrals are comparable, for the same number of parameters varied, to those obtained in Table IX. Adding the two-parameter and four-parameter monopole terms to the Talmi-integral parameterization generally gives only a marginally better χ value than is obtained by incorporating the next higher terms in the Talmi sequence. Setting the values of the Talmi integrals that are not varied equal to the G-matrix values, or leaving them out entirely, generally does not influence the fits significantly. This is true for each of the components studied.

For the tensor component, the χ value obtained with the Talmi-integral approach improves only slightly in going beyond the first two parameters. The four-parameter fits in Tables VII and X give very similar results. Comparing the results of the spin–orbit fits in Tables VII and XI, we see that the Talmi-integral fits are slightly better than the density-independent fits of Table XI.

These results indicate that the Talmi-integral parameterization and potential-model parameterizations can give results of comparable quality for the same number of parameters varied. However, we favor the potential-model parameterizations because they can be more easily extrapolated to other mass regions and can be more readily related to the underlying physics.

IV.B. *Simple Interactions*

Table VIII contains the results of fits in which the strengths of the central components of some of the conventional simple interactions were varied while the tensor and spin–orbit components of the interaction were either set to zero, held fixed at the HKT interaction values, or allowed to vary model independently. We consider the (density-independent) delta interaction (δ), and the surface-delta interaction (SDI) combined with the C2 and C4 monopole terms (see Table VI). The SDI, C2 interaction corresponds to the usual "modified surface-delta" interaction (Ref. [7]) which includes the isospin-dependent monopole term.

It is evident from Table VIII that most of the χ values obtained with the central components derived from the delta and surface-delta interactions, with or without additional monopole terms, are generally large compared to the model-independent results discussed in Section IV.A. The best χ is obtained for the SDI, C4 parameterization. The χ value of 1.92 in this case compares favorably with the model-independent value of 1.19, particularly in terms of economy of central parameters used (6 versus 20). This suggests that a somewhat more sophisticated central component, with only a few more parameters, may be adequate. The significant improvement of the surface-delta ($\chi = 1.92$) over the (density-independent) delta interaction ($\chi = 3.32$) is another indication of the importance of density dependence. It also appears that fixing the spin–orbit and tensor components at their bare G-matrix values does not produce any gain relative to leaving them out altogether. To improve the fit, the spin–orbit and tensor parameters must be varied.

IV.C. OBEP *and Multipole Interactions*

A wide variety of parameter spaces has been explored for the central, tensor, and spin–orbit components. A selection of these for the central component are given in Table IX. The benchmarks for the χ values are obtained by (a) setting the central component equal to zero ($\chi = 20.6$) and (b) the model-independent (MI) 20-parameter (WNOALS) central interaction ($\chi = 1.19$). (In both cases all 27 parameters of the tensor and spin–orbit components were varied using the MI spin-tensor decomposition method.)

We consider in general only up to 12-parameter fits, three for each of the four channels. Three is in fact the maximum allowed for the $(S, T) = (0, 0)$ and $(1, 1)$ channels (see Table IV). However, for both of these channels and, in particular for the $(S, T) = (0, 0)$ channel, we find that all three parameters cannot be meaningfully determined. That is, when there are three parameters, the error in all three is extremely large; when there are only two parameters, the error is usually more reasonable; and when there is one parameter the error is always small. As a consequence of this fact, the χ value is essentially the same for the DD, C4 12-parameter fits and the DD, C2 10-parameter fits shown in Table IX. Even though in principle we could go up to seven parameters each for the $(S, T) = (0, 1)$ and $(1, 0)$ channels, we have found no significant decrease in the χ value when going beyond three parameters.

Everything else being equal, the density-dependent interaction almost always does better than the corresponding density-independent interaction. As mentioned in Section III.B, we have assumed a "surface" form for the density-dependent interaction obtained with $A_d = -1$ in Eq. (26). Also, we note that the four-parameter (C4) monopole always does somewhat better than the two-parameter (C2) monopole (with the exception of the case when there are a total of 12 parameters, as discussed in the above paragraph).

The OPEP part of the interaction is presumably the best understood component of the nucleon–nucleon potential. Since it is the longest ranged mesonic-exchange component it should not be affected much by short-range correlations. Furthermore, since the density dependence is often regarded as a consequence of the nuclear medium modification of the short-range interactions (Ref. [30]), the OPEP should again be least affected. Thus, we have carried out several least-squares fits with the longest ranged term fixed at the standard density-independent OPEP form; these are denoted by FOPEP in the tables. It is encouraging to note that everything else being the same, the χ value is improved when the OPEP term is added in with a fixed strength.

Several of the density-dependent fits with 12 parameters give values of χ in the range of 1.35 which compare favorably with the "best" value of 1.19. However, the results are not unique: $\chi = 1.45$ with C4, Q4, H4 (only multipole terms); $\chi = 1.35$ for three Yukawas; $\chi = 1.32$ for two Yukawas plus FOPEP plus the C4 monopole.

The choice of our "best-fit" interaction is based upon the consideration of economy, that is, a reasonably small χ value for a relatively small number of

parameters, and universality, that is, the extent to which the interaction might be used directly with a different model space in a different region of nuclei.

Even though the multipole interaction provides a reasonable 12-parameter fit for the *sd* shell, it is difficult to extrapolate the *sd*-shell results to other mass regions. In order to reproduce the core-polarization correction it appears that all multipoles are important (Refs. [41, 42, 39]). The *sd* shell allows only multipoles up to $L=4$. For the *fp* shell, multipoles up to $L=6$ are allowed, and much higher values are needed for heavy nuclei. Thus, in order to apply the empirical *sd*-shell multipole interaction to heavier nuclei, we need to know how to extrapolate the strengths for the $L=0$, 2, and 4 multipoles and how to introduce the higher multipole terms.

For the "best" central interaction we choose the 8-parameter C4, M4, FOPEP fit. It gives a χ value of 1.42 which is only marginally worse than the best 12-parameter fit. (The medium-ranged Yukawa is arbitrarily chosen over the equally good fit with the short-ranged Yukawa.) Perhaps at best, the monopole parameters would need to be readjusted in another model space, and at worst all eight parameters may need to be readjusted.

Fits similar to the ones discussed above for the central component were carried out for the tensor and spin–orbit components separately, and the results are shown Tables X and XI, respectively. For the tensor component, the inclusion of a density dependence does not lead to a significant improvement in the fit. This is in contrast to the spin–orbit component, where a systematic reduction in the χ values is very noticeable. The best fit in the tensor component is the density-dependent four-parameter fit for the isoscalar and isovector channels where the strengths for both the short and the long ranges were varied. Hence these parameters were also a natural choice for the "best-fit" interaction. For the spin–orbit component, the four-parameter density-dependent fit with the short and medium ranges is only marginally better than the two-parameter density-dependent fit for the medium range. Thus from the point of view of economy, the latter form was selected for the "best-fit" interaction.

IV.D. *The "Best-Fit" Interaction*

The remaining discussions in this paper are based on one particular combination of parameter choices which we believe combines elements of quality and simplicity. This interaction has a total of 14 two-body potential parameters and will be referred to as the "best-fit" interaction. It consists of the following elements:

(a) for the central component (eight parameters); the four-parameter monopole terms (C4) plus the four-parameter density-dependent (DD) medium-ranged Yukawa terms (M4) plus density-independent long-ranged Yukawa terms with the strengths fixed at the OPEP values (FOPEP),

(b) for the tensor component (four parameters); the two-parameter DD short-ranged OBEP terms (S2) plus the two-parameter DD long-ranged OBEP terms (L2),

(c) for the spin–orbit component (two parameters); the two-parameter DD short-ranged OBEP terms (S2), and

(d) zero for the ALS component.

Together with the three single-particle energies, this provides an interaction with a total of 17 parameters. The χ value for this fit is 1.66, a value which is close to that expected from the discussions of the individual components in Section IV.C.

With this form for the "best-fit" interaction we next examine the dependencies upon some of the variables in the calculation that up to now have been assumed to be fixed.

(1) *Mass dependence of the* TBME. Table XII gives the χ value for the 17-parameter "best-fit" interaction as a function of the power P for the assumed mass dependence of the TBME expressed in the form

$$\langle V\rangle(A) = \langle V\rangle(A=18)(A/18)^{-P}. \tag{35}$$

There is a shallow minimum with $\chi = 1.61$ around $P = 0.35$. According to the discussion under point (3) in Section II.C this value of P is still reasonable, and in the remaining discussion we will take $P = 0.35$ for the "best-fit" interaction. The 17 parameters of this interaction (SDPOTA) are given in Table XIII.

(2) *Mass dependence of the* SPE. Until now we have assumed, for the reasons indicated in point (4) of Section II.C, that the SPE are constant as a function of mass. The "best fit" was repeated by introducing linear mass-dependent SPE of the form

$$\mathrm{SPE}(A) = \mathrm{SPE}(A=17) + [(A-17)/22][\mathrm{SPE}(A=39) - \mathrm{SPE}(A=17)]$$

for each of the three SPE ($0d_{5/2}$, $1s_{1/2}$, and $0d_{3/2}$). This 20-parameter fit gave $\chi = 1.46$, which is a moderate reduction from the value of $\chi = 1.61$ obtained with no SPE mass dependence. The 20 parameters of this interaction (SDPOTB) are given in Table XIII. [We remind the reader that these "$A = 39$" SPE represent the kinetic

TABLE XII

The χ Value for the "Best-fit" 17-Parameter Interaction as a Function of the Power Assumed for the Mass Dependence of the TBME

P	X
0.25	1.76
0.30	1.66
0.35	1.61
0.40	1.61
0.45	1.67
0.50	1.78

TABLE XIII

Parameter Values for the "Best-Fit" Interactions with $P = 0.35$ for the TBME Mass Dependence

Interaction					SDPOTA	SDPOTB	SDPOTB
Number of parameters					17	20	20
					Parameter value (MeV)		Error(MeV)[b]
SPE($A=17$)	$0d_{5/2}$				−4.0003	−4.0800	0.022
	$1s_{1/2}$				−3.4512	−3.1119	0.070
	$0d_{3/2}$				1.6791	1.8245	0.130
SPE($A=39$)	$0d_{5/2}$				0.	0.418	0.320
−SPE($A=17$)	$1s_{1/2}$				0.	−0.678	0.300
	$0d_{3/2}$				0.	−0.330	0.210
Component	S	T	Form	Range (fm)			
Central	0	0	C		0.7454	0.6993	0.33
			DD-M	0.50	−1761.	−2808.	480.
			DI-L	1.414	31.389	31.389	[a]
	1	0	C		−1.9624	−1.8741	0.078
			DD-M	0.50	−462.9	−461.1	15.
			DI-L	1.414	−10.463	−10.463	[a]
	0	1	C		0.2430	0.1414	0.075
			DD-M	0.50	−493.6	−485.6	12.
			DI-L	1.414	−10.463	−10.463	[a]
	1	1	C		0.6562	0.7120	0.062
			DD-M	0.50	−454.3	−486.7	80.
			DI-L	1.414	3.488	3.488	[a]
Tensor	1	0	DD-S	0.25	−18400.	−26200.	3000.
			DD-L	1.414	10.57	16.25	3.0
	1	1	DD-S	0.25	6780.	197.0	3400.
			DD-L	1.414	−9.28	−3.80	3.0
Spin–orbit	1	0	DD-S	0.25	−37000.	−251000.	48000.
	1	1	DD-S	0.25	−60600.	−59800.	2100.

[a] These terms where held fixed in the fit.

[b] The errors in the 17-parameter fit are similar to or slightly smaller than those given here for the 20-parameter fit.

energy plus the interaction between nucleons in the *sd*-shell with those in the $0s$ and $0p$ closed shells. The total binding energies of the $A = 39$ (and $A = 40$) nuclei are obtained from these "$A = 39$" SPE plus the contribution from the interactions between nucleons in the *sd* shell.] The fitted mass dependence of the SPE turns out to be relatively small. We are not aware of any estimates, for example, based on a Hartree–Fock calculation, as to how large this mass dependence should be.

(3) *Parameters of the density dependence.* Here we consider the sentitivity of χ to the parameters of the density dependence, namely, A_d, B_d, R_0, and a in Eq. (26).

Variation of A_d provides the most dramatic dependence. The χ values as a function of A_d for the SDPOTA interaction are given in Table XIV. The minimum of $\chi = 1.61$ occurs at $A_d = -1.0$, which corresponds to a density dependence with the interaction going to zero in the nuclear interior, and goes up to $\chi = 3.28$ for $A_d = 0$, which corresponds to no density dependence. Our initial choice of $A_d = -1$ was motivated by a preliminary knowledge of this fact together with the previously known successes of the "surface-delta" type interactions.

Variation of the remaining three parameters seems to provide a fine-tuning of the density dependence which can lower the χ value down to about 1.40. This can be achieved in a variety of ways: by decreasing the power B_d, by increasing the radius R_0, by decreasing the diffuseness a, or by some combination of these. The related significance of all of these variations can be qualitatively understood by means of Table V and the discussion in Section III.B. It can be seen from the table that the $0d$–$1s$–$1s$–$1s$ and $1s$–$1s$–$1s$–$1s$ matrix elements are the most sensitive to the density dependence. For all of the optimal ($\chi \approx 1.40$) parameterizations of $D(R)$, the integral in Eq. (26) gives -0.70 to -0.80 for the $0d$–$1s$–$1s$–$1s$ to $0d$–$0d$–$0d$–$0d$ ratio and 0.70 to 0.86 for the $1s$–$1s$–$1s$–$1s$ to $0d$–$0d$–$0d$–$0d$ ratio. We conclude that our initial parameterization of the density dependence is adequate and cannot be significantly tested or improved upon in a unique way from consideration of the sd-shell data alone.

Within our chosen "best-fit" parameterizations there are two measures of the uncertainties of the individual strength parameters. The first is the uncorrelated error obtained from the fit; these are given for the 20-parameter fit in the last column of Table XIII. (These include the usual multiplication by χ.) Another is the variation in the parameter values between SDPOTA and SDPOTB interactions listed in the table. Overall, these two measures agree. It is clear that some of the parameters are much more poorly determined than others, in particular those for the $(S, T) = (0, 0)$ central channel, the $(S, T) = (1, 1)$ tensor channel, and the $(S, T) = (1, 0)$ spin–orbit channel. The parameters in these channels appear to be

TABLE XIV

The χ Value for the SDPOTA Interaction as a Function of A_d in Eq. (26)

A_d	χ
−1.2	2.04
−1.1	1.69
−1.0	1.61
−0.9	1.70
−0.8	1.87
−0.6	2.28
−0.4	2.66
−0.2	3.00
0.0	3.28

correlated with each other, and some linear combinations may be better determined.

In Fig. 7 the spin-tensor components of the SDPOTA and SDPOTB interactions are compared with those of the WNOALS interaction. The sensitivity of the matrix elements to the strengths of the potential can be inferred from a comparison of the two sets of matrix elements in Fig. 7 with corresponding interaction strengths in Table XIII. It can be seen in Fig. 7 that the empirical WNOALS central values are

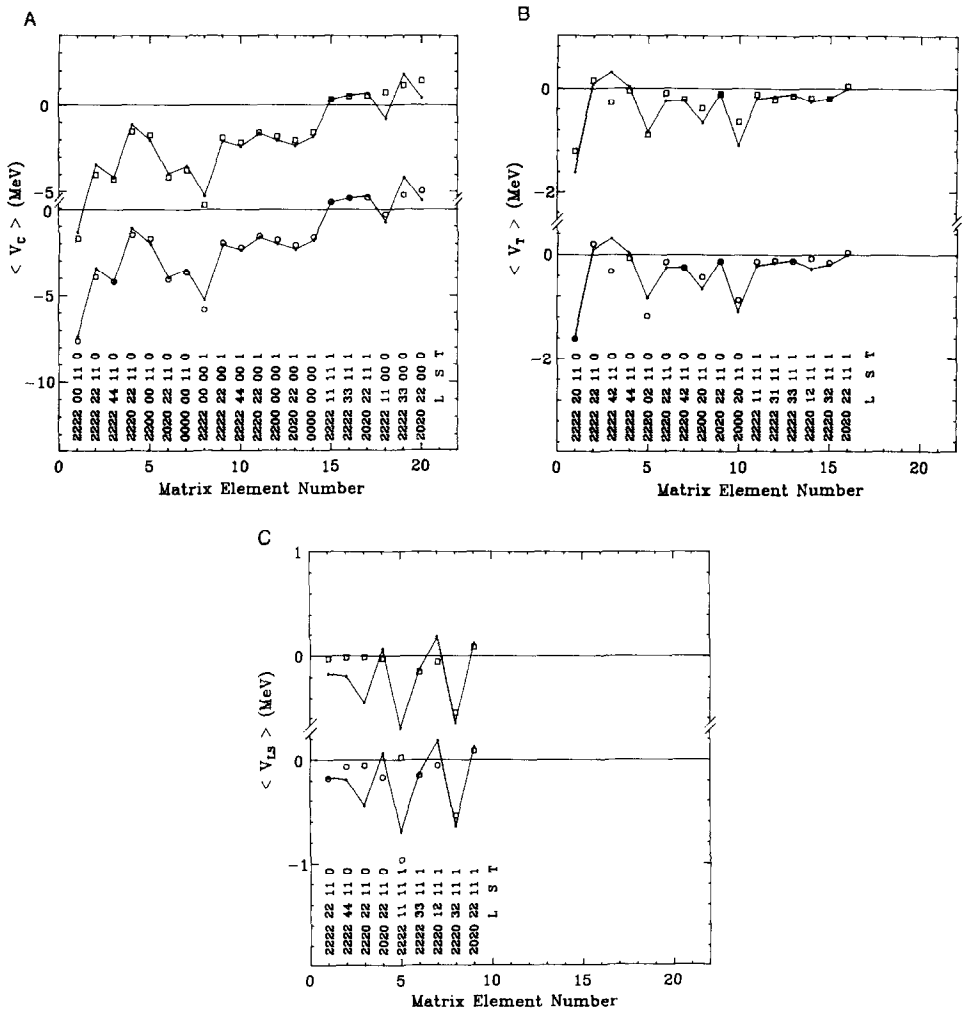

FIG. 7. (A) Matrix elements for the central component. In the top panel the WNOALS TBME are compared with those from the 17-parameter "best-fit" interaction. In the bottom panel the WNOALS TBME are compared with those from the 20-parameter "best-fit" interaction which includes the mass-dependent SPE. (B) Matrix elements for the tensor component. The same interactions as those in (A) are compared and the conventions are the same. (C) Matrix elements for the spin–orbit component. The same interactions as those in (A) are compared and the conventions are the same.

particularly well reproduced with our potential model. This is also generally true for the tensor components. For the spin–orbit interaction our $(L, S, T) = (1, 1, 1)$ matrix element is noticeably larger than WNOALS, and one of the $(2, 1, 0)$ matrix elements is noticeably smaller; however, the general trend is very similar.

V. Summary and Conclusion

In this work, we have compared a large variety of model-independent and semi-empirical parameterizations for the effective interactions with regard to experimental binding-energy data in the *sd* shell. Detailed comparisons are made throughout the paper. We list the main conclusions:

(1) The antisymmetric spin–orbit (ALS) component is relatively unimportant and poorly determined compared to the central, tensor, and spin–orbit components.

(2) In the model-independent parameterizations there are many linear combinations of parameters which are poorly determined. It is important to replace these with those obtained from some realistic interaction. Any realistic bare G-matrix appears to be adequate, and, in particular, the OBEP parameterizations such as those of Hosaka *et al.* are easy to evaluate.

(3) The Talmi-integral parameterizations are only marginally less successful than the more general model-independent (TBME) parameterizations.

(4) The one-pion-exchange potential (OPEP) always improves the fit when it is introduced at the standard fixed strength in the central component. On the other hand, for the tensor component the introduction of a fixed strength OPEP worsens the fit.

(5) We have found some simple potential-model parameterizations which reproduce he *sd*-shell data with an rms deviation which is smaller than that obtained in a model-independent fit which uses the same number of parameters and which replaces the poorly determined linear combinations with G-matrix values.

(6) An essential ingredient of these potential models is the density dependence. The optimal choice seems to be an interaction which goes to zero in the nuclear interior. At the most general level, this density dependence improves the results obtained with the Talmi-integral parameterizations. It also improves the results obtained with potential-model parameterizations.

In regard to point (5) we have chosen the "best-fit" interaction (SDPOTA) discussed in Section IV.D. With 14 TBME parameters and six SPE parameters the interaction reproduces the 447 *sd*-shell binding-energy data to within an rms deviation between experiment and theory of about 260 keV as compared to about 185 keV in the case of the model-independent 66-parameter fit. As an example of the comparison between interactions, we show in Fig. 8 the experimental energy levels of ^{22}Na compared to those obtained with several of the interactions discussed in this paper and in Ref. [16]—from left to right: (SKSP4) a recent "no-parameter"

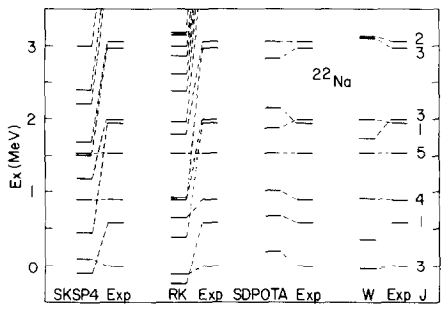

FIG. 8. Experimental low-lying $T=0$ states of ^{22}Na compared with those based on three interactions: (SKSP4) the renormalized G-matrix of Shurpin, Kuo, and Strottman, (Ref. [2]) based on the Paris potential (as taken from Fig. 18 of their paper); (RK) the renormalized G-matrix of Kuo (Ref. [19]); (SDPOTA) the present "best-fit" interaction given in Table XIII; and (W) the 47-parameter interaction of Wildenthal (Ref. [5]). The levels are plotted relative to the $J=5$ state.

calculation based on a renormalized G-matrix obtained with the Paris potential (Ref. [43]); (RK) the original renormalized G-matrix of Kuo; (SDPOTA) our 17-parameter "best-fit" interaction; and (W) the W interaction.

We propose that these potential-model parameterizations may be a useful way to improve calculations for heavier nuclei. The parameters in such a model may be model-space and mass dependent and should in general be treated as free parameters in each case. We have initiated such investigations for the $0p$ and $0f1p$ model spaces (Ref. [44]).

The mass dependence of the potential parameters may turn out to be simple, and ultimately one would like to have a unified approach for all nuclei. This was the approach of Schiffer and True (Ref. [33]) who used a mass-independent potential model to analyze diagonal two-body matrix elements which connect a wide variety of shell-model orbitals (over a wide mass region). In contrast to this, we have analyzed both diagonal and off-diagonal two-body matrix elements which connect a few orbitals (over a relatively small mass region). The next step would be to try to combine these two types of data sets. In addition, one could consider combining binding-energy data for the $0p$ and $0f$–$1p$ shells with the sd-shell data. Such combined analyses are currently under way (Ref. [44]). Including magnetic moments in the fits is another interesting possibility (Ref. [45]). It would also be interesting to use these types of interactions in Hartree–Fock calculations for properties of closed-shell nuclei.

ACKNOWLEDGMENTS

W. R. and R. J. acknowledge the hospitality and support of the National Superconducting Cyclotron Laboratory, Michigan. B. A. B. acknowledges the hospitality and support of the University of Stellenbosh, the Council for Scientific and Industrial Research, the University of Cape Town, and the University of the Western Cape, Republic of South Africa. This work was supported in part by National Science Foundation Grants PHY83–12245 and PHY87-18772.

REFERENCES

1. T. T. S. KUO, *Annu. Rev. Nucl. Sci.* **24** (1974), 101.
2. J. SHURPIN, T. T. S. KUO AND D. STROTTMAN, *Nucl. Phys. A* **408** (1983), 310.
3. E. C. HALBERT, J. B. MCGRORY, B. H. WILDENTHAL, AND S. P. PANDYA, "Ad. in Nucl. Phys." (M. Baranger and E. Vogt, Eds.), Vol. 4, p. 315, Plenum, New York, 1971.
4. J. B. MCGRORY AND B. H. WILDENTHAL, *Annu. Rev. Nucl. Part. Sci.* **30** (1980), 383.
5. B. H. WILDENTHAL, "Progress in Particle and Nuclear Physics" (D. H. Wilkinson, Ed.), Vol. 11, p. 5, Pergamon, Oxford, 1984.
6. A. HOSAKA, K. I. KUBO, AND H. TOKI, *Nucl. Phys. A* **444** (1985), 76. Note the following corrections: in Eq. (2) the σ should be replaced by **s**, in Eq. (3) the $Y_{LS}(x)$ term should have the factor e^{-x}/x^2 in place of e^{-x}/x, and in Table 3 the range should be 0.40 rather than 0.50.
7. P. J. BRUSSAARD AND P. W. M. GLAUDEMANS, "Shell Model Applications in Nuclear Spectroscopy," North-Holland, Amsterdam, 1977.
8. W. CHUNG, Ph.D. thesis, Michigan State University, 1976; B. H. WILDENTHAL, Lectures presented at the conference on "Elementary Modes of Excitation in Nuclei" (R. Broglia and A. Bohr, Eds.), Soc. Italiana de Fisica, 1977.
9. J. D. MCCULLEN, B. F. BAYMAN, AND L. ZAMICK, *Phys. Rev.* **134** (1964), B515.
10. W. KUTSCHERA, B. A. BROWN, AND K. OGAWA, *Riv. Nuovo Cimento Ser.* 3, **1**, No. 12 (1978), 1.
11. S. COHEN AND D. KURATH, *Nucl. Phys.* (1965), 73.
12. J. P. ELLIOTT, A. D. JACKSON, H. A. MAVROMANTIS, E. A. SANDERSON, AND B. SINGH, *Nucl. Phys. A* **121** (1968), 241.
13. M. W. KIRSON, *Phys. Lett. B* **47** (1973), 110.
14. K. YORO, *Nucl. Phys. A* **333** (1980), 67.
15. K. KLINGENBECK, W. KNUPFER, M. G. HUBER, AND P. W. M. GLAUDEMANS, *Phys. Rev. C* **15** (1977), 1483.
16. B. A. BROWN, W. A. RICHTER, AND B. H. WILDENTHAL, *J. Phys. G* **11** (1985), 1191. The scale of the matrix elements in Fig. 2 should be reduced by three and the scale of the matrix elements in Figs. 3 and 4 should be divided by four. Equation (2) of the text should be replaced by Eq. (11) of the present work.
17. R. D. LAWSON, "Theory of the Nuclear Shell Model," Oxford Univ. Press (Clarendon), Oxford, 1980.
18. B. H. WILDENTHAL, unpublished.
19. T. T. S. KUO, *Nucl. Phys. A* **103** (1967), 71.
20. K. ANDO, H. BANDO, AND E. M. KRENCIGLOWA, *Prog. Theor. Phys.* Suppl. 65 (1979), 38.
21. K. YOSHINADA, *Phys. Rev. C* **26** (1982), 1784.
22. G. A. TIMMER, R. VAN DER HEYDEN, B. C. METSCH, AND K. KLINGENBECK, *Phys. Lett. B* **82** (1979), 305.
23. B. C. METSCH, G. A. TIMMER, R. VAN DER HEYDEN, AND P. W. M. GLAUDEMANS, *Z. Phys. A* **306** (1982), 105.
24. NGUYEN VAN GIAI AND H. SAGAWA, *Phys. Lett. B* **106** (1981), 379.
25. J. DECHARGE AND D. GOGNY, *Phys. Rev. C* **21** (1980), 1568.
26. J. FRIEDRICH AND P. G. REINHARD, *Phys. Rev. C* **33** (1986), 335.
27. P. W. M. GLAUDEMANS, P. J. BRUSSAARD, AND B. H. WILDENTHAL, *Nucl. Phys. A* **102** (1967), 593.
28. A. B. MIGDAL, "Nuclear Theory; The Quasiparticle Method," Benjamin, New York, 1968; "Theory of Finite Fermi Systems and Applications to Atomic Nuclei," Wiley, New York, 1967.
29. J. W. NEGELE, *Phys. Rev. C* **1**, 1260 (1970).
30. M. R. ANASTASIO, L. S. CELENZA, W. S. PONG, AND C. M. SHAKIN, *Phys. Rep.* **100** (1983), 328; L. S. CELEMZA, W. S. PONG, AND C. M. SHAKIN, *Phys. Rev. Lett.* **47** (1981), 3.
31. D. VAUTHERIN AND D. M. BRINK, *Phys. Rev. C* **5** (1972), 626 .
32. T. A. BRODY AND M. MOSHINSKY, "Tables of Transformation Brackets for Nuclear Shell-Model Calculations," Monografias del Instituto de Fisica, Mexico, 1969.

33. J. P. SCHIFFER AND W. T. TRUE, *Rev. Mod. Phys.* **48** (1976), 191.
34. H. SAGAWA, B. A. BROWN, AND O. SCHOLTEN, *Phys. Lett. B* 159 (1985), 228.
35. G. F. BERTSCH, J. BORYSOWICZ, H. MCMANUS, AND W. G. LOVE, *Nucl. Phys. A* **284** (1977), 399.
36. N. ANANTARAMAN, H. TOKI, AND G. F. BERTSCH, *Nucl. Phys. A* **398** (1983), 296.
37. R. BRYAN AND B. L. SCOTT, *Phys. Rev. C* **177** (1969), 1435.
38. M. LACOMBE, B. LOISEAU, J. M. RICHARD, R. VINH MAU, J. COTE, P. PIRES, AND R. DE TOURREIL *Phys. Rev. C* **21** (1980), 861.
39. G. H. HERLING AND T. T. S. KUO, *Nucl. Phys. A* **181** (1972), 113.
40. L. J. TASSIE AND F. C. BARKER, *Phys. Rev.* **111** (1958), 940.
41. G. F. BERTSCH, *Nucl. Phys.* **74** (1965), 234.
42. G. E. BROWN AND T. T. S. KUO, *Nucl. Phys. A* **92** (1967), 481.
43. J. SHURPIN, T. T. S. KUO, AND D. STROTTMAN, *Nucl. Phys. A* **408** (1983), 310.
44. W. A. RICHTER, R. E. JULIES, AND B. A. BROWN, unpublished.
45. A. G. M. VAN HEES, A. A. WOLTERS, AND P. W. M. GLAUDEMANS, *Phys. Lett. B* **196** (1987), 1.